AD-A194 718 LAGRANGIAN ANALYSIS(U) CALIFORNIA RESEARCH AND 1/1
TECHNOLOGY INC ALBUQUERQUE NM G M LLOYD ET AL.
01 MAR 87 CRTA-TR-3950-1 DNA-TR-87-145 DNA001-86-C-0148
UNCLASSIFIED F/G 19/1 NL

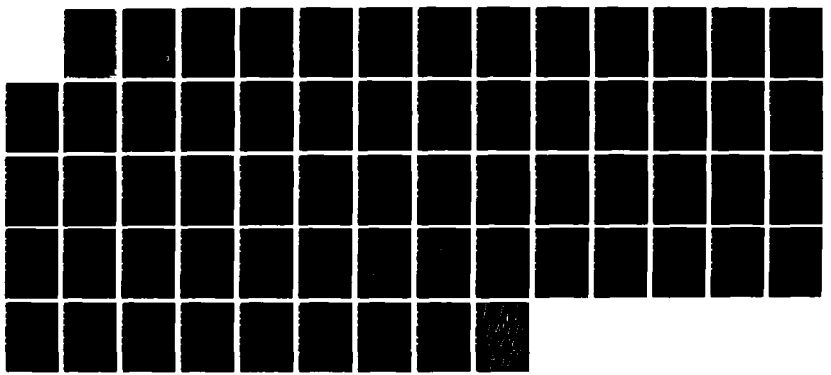

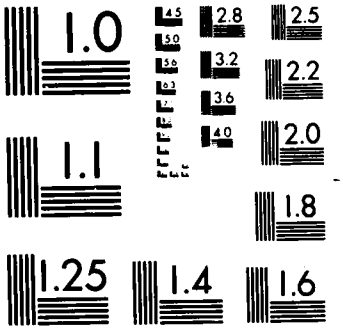
1.0
1.1
1.25
1.4
1.6
1.8
2.0
2.2
2.5
2.8
3.2
3.6
4.0
4.5
5.0
5.6
6.3
7.1

DNA-TR-87-145

LAGRANGIAN ANALYSIS

G. M. Lloyd
E. J. Rinehart
California Research & Technology, Inc.
2017 Yale Boulevard SE
Albuquerque, NM 87106

1 March 1987

Technical Report

CONTRACT No. DNA 001-86-C-0148

THIS WORK WAS SPONSORED BY THE DEFENSE NUCLEAR AGENCY
UNDER RDT&E RMC CODE B4662 D RS RB 00055 25904D.

Prepared for
Director
DEFENSE NUCLEAR AGENCY
Washington, DC 20305-1000

Destroy this report when it is no longer needed. Do not return to sender.

PLEASE NOTIFY THE DEFENSE NUCLEAR AGENCY ATTN: TITL, WASHINGTON, DC 20305 1000, IF YOUR ADDRESS IS INCORRECT, IF YOU WISH IT DELETED FROM THE DISTRIBUTION LIST, OR IF THE ADDRESSEE IS NO LONGER EMPLOYED BY YOUR ORGANIZATION.

DISTRIBUTION LIST UPDATE

This mailer is provided to enable DNA to maintain current distribution lists for reports. We would appreciate your providing the requested information.

☐ Add the individual listed to your distribution list.

☐ Delete the cited organization/individual.

☐ Change of address.

NAME: _____

ORGANIZATION: _____

OLD ADDRESS	CURRENT ADDRESS
_____	_____
_____	_____
_____	_____

TELEPHONE NUMBER: ( ) _____

SUBJECT AREA(s) OF INTEREST:

_____ _____

_____ _____

_____ _____

DNA OR OTHER GOVERNMENT CONTRACT NUMBER: _____

CERTIFICATION OF NEED-TO-KNOW BY GOVERNMENT SPONSOR (if other than DNA):

SPONSORING ORGANIZATION: _____

CONTRACTING OFFICER OR REPRESENTATIVE: _____

SIGNATURE: _____

CUT HERE AND RETURN

Director
Defense Nuclear Agency
ATTN: TITL
Washington, DC 20305-1000

Director
Defense Nuclear Agency
ATTN: TITL
Washington, DC 20305-1000

REPORT DOCUMENTATION PAGE

1a REPORT SECURITY CLASSIFICATION UNCLASSIFIED	1b RESTRICTIVE MARKINGS
2a SECURITY CLASSIFICATION AUTHORITY N/A since Unclassified	3 DISTRIBUTION/AVAILABILITY OF REPORT Approved for public release; distribution is unlimited.
2b DECLASSIFICATION/DOWNGRADING SCHEDULE N/A since Unclassified	
4 PERFORMING ORGANIZATION REPORT NUMBER(S) CRTA-TR-3950-1	5 MONITORING ORGANIZATION REPORT NUMBER(S) DNA-TR-87-145
6a NAME OF PERFORMING ORGANIZATION California Research & Technology, Inc. 6b OFFICE SYMBOL (If applicable)	7a NAME OF MONITORING ORGANIZATION Director Defense Nuclear Agency
6c ADDRESS (City, State, and ZIP Code) 2017 Yale Boulevard SE Albuquerque, NM 87106	7b ADDRESS (City, State, and ZIP Code) Washington, DC 20305-1000
8a NAME OF FUNDING/SPONSORING ORGANIZATION 8b OFFICE SYMBOL (If applicable) SPSS/Canada	9 PROCUREMENT INSTRUMENT IDENTIFICATION NUMBER DNA 001-86-C-0148
8c ADDRESS (City, State, and ZIP Code)	10 SOURCE OF FUNDING NUMBERS PROGRAM ELEMENT NO: 62715H; PROJECT NO: RS; TASK NO: RB; WORK UNIT ACCESSION NO: DH018220

11 TITLE (Include Security Classification)

LAGRANGIAN ANALYSIS

12 PERSONAL AUTHOR(S)
Lloyd, George M.; Rinehart, Eric J.

13a TYPE OF REPORT	13b TIME COVERED	14 DATE OF REPORT (Year, Month, Day)	15 PAGE COUNT
Technical	FROM 861201 TO 870301	870301	60

16 SUPPLEMENTARY NOTATION
This work was sponsored by the Defense Nuclear Agency under RDT&E RMC Code B4662 D RS RB 00055 25904D.

17 COSATI CODES			18 SUBJECT TERMS (Continue on reverse if necessary and identify by block number)
FIELD	GROUP	SUB-GROUP	Material Models; Lagrangian Analysis; Constitutive Relationships,
	1		

19 ABSTRACT (Continue on reverse if necessary and identify by block number)

Estimation of stress and strain paths followed in in situ, high explosive field tests may be obtained from direct inversion of the velocity and stress histories measured. When the field tests are designed as one-dimensional tests (planar, cylindrical, or spherical), a technique commonly called Lagrangian Analysis of Stress and Strain (LASS) has been employed. The results from recent LASS analysis of dry soils have not been self-consistent nor yielded estimates which have been shown to be better than currently arrived at by lab tests and parametric calculations.

This report develops another method of LASS which deviates somewhat from earlier "path-line" and "traveling wave" formulations. Equations for the new method are derived. Estimates due to instrumentation inaccuracy are examined. Methodological errors in estimation of strains and stress bounds are also investigated.

20 DISTRIBUTION/AVAILABILITY OF ABSTRACT ☐ UNCLASSIFIED/UNLIMITED ☒ SAME AS RPT ☐ DTIC USERS	21 ABSTRACT SECURITY CLASSIFICATION UNCLASSIFIED
22a NAME OF RESPONSIBLE INDIVIDUAL Sandra E. Young	22b TELEPHONE (Include Area Code) (202) 325-7042 22c OFFICE SYMBOL DNA/CSTI

DD FORM 1473, 84 MAR — 83 APR edition may be used until exhausted. All other editions are obsolete.

19. ABSTRACT (Continued)

While this paper does not address all the possible sources of inconsistency, it will point out many which have not received attention before. Specifically,

1. Errors due to instrumentation inaccuracy.

2. Methodological errors in estimation of strains and stress bounds.

SUMMARY

A set of algorithms has been developed for the estimation of strain-time histories in 1-D spherical fields. Methods for the estimation of stress-difference and stress-bounds have also been developed. Qualitative statements regarding the effects of possible errors in method and instrument measurement error have been made and substantiated.

Further:

1. At the current state-of-the-art, Lagrangian analysis must be considered as an adjunct to laboratory methods and parametric calculations in the development of better material models.

2. The methods outlined in this paper require no explicit shape function to be assumed. Thus, complex flow fields can be dealt with.

3. Accuracy of strain-time histories are affected to first order by errors in late-time displacement (as due, in practice, to baseline shifts, instrument calibration, and/or accuracy).

4. Although only briefly discussed here, we reiterate a known result: stress-difference time history estimation is very sensitive to errors in acceleration and $\partial\sigma_r/\partial h$.

5. Local estimates of time of arrival and flow surface should be used in estimating strains, unless errors in gage surveying or gage availability dictate otherwise.

6. A more global estimate of time of arrival and flow surface should be used in estimating stress-bounds in order to avoid extrapolation.

7. Practically, difficulty still remains in validating the degree of one-dimensionality of the in situ environment. Because the state of current instrumentation does not allow a measure of the uncertainty, the only clear (but by no means unequivocal or definitive) method would seem to be analysis of a corresponding two- or three-dimensional calculation.

8. Difficulties and ambiguities in validating measurements from current motion and stress must be dealt with in order to remove possible first order errors from strain estimates.

CONVERSION FACTORS, NON-SI TO SI (METRIC) UNITS OF MEASUREMENT

Non-SI units of measurement used in this report can be converted to SI (metric) units as follows:

Multiply	By	To Obtain
degrees (angle)	0.01745329	radians
feet	0.3048	meters
gallons (US liquid)	3.785412	cubic decimeters (liters)
inches	2.54	centimeters
kips (force)	4.448222	kilonewtons
kips (force per square inch)	6.894757	megapascals
megatons (nuclear equivalent of TNT)	4.184	petajoules
pounds (force) per square inch	6.894757	kilopascals
pounds (mass)	0.4535924	kilograms
pounds (mass) per cubic foot	16.01846	kilograms per cubic meter
kbars	98	megapascals
feet	1/.3048	meters

TABLE OF CONTENTS

LIST OF ILLUSTRATIONS

SECTION 1
INTRODUCTION

Estimation of stress and strain paths followed in geological media using measured velocity and stress gages obtained from purely one-dimensional events, a technique commonly called Lagrangian Analysis of Stress and Strain (LASS), has been employed for at least 15 years (Refs. 1, 2, 3, 4, 5, 6). Currently, such techniques are being used to provide insight into the information needed to construct, ideally, more precise material models for use in 2-D finite difference calculations.

The results from recent LASS analysis of dry soils to date have not been self-consistent nor yielded models which have been shown to be better than those currently arrived at by laboratory tests and parametric calculations. The reason for this is twofold:

First, it is due to the inability to validate motion and stress measurements to the required degree of precision required, resulting from:

1. Lack of repeatability for similarly emplaced gages.

2. Imprecisely defined arrival and rise times.

3. Inadequate calibration techniques.

4. Inability to objectively correct for gage drift after shock passage.

5. Inability to measure "hoop" stresses.

6. Limited survivability hampering validation.

7. Limited validation of geometrical symmetries required for analysis.

8. Inconsistencies between motion and stress measurements, partly due to inaccurate early-time response of stress gages.

Second, it is because very little has been done regarding the influences of possible systematic and inherent errors and errors due to varying judgment as to what constitutes a "good" data set and appropriate methods of data reduction. For example, separate LASS analyses of gorund motion data from event MP2 (Refs. 7 & 8), by Trulio, (Ref. 9), and Allen (Ref. 10) came to remarkably differing conclusions regarding suitability of current models.

This paper develops another method of Lagrangian analysis, which deviates somewhat from earlier "path-line" (Refs. 1, 2, 3, 4, 5, 6) and "traveling wave" formulations. The method may be considered as computationally simplifying the path line method (Refs. 1 and 3) in that directional derivatives along an arbitrary path are replaced by partial derivatives related to the time-of-arrival. It may also be considered a generalization of the traveling wave method (Refs. 4 and 5), applicable for arbitrarily complicated one-dimensional flow.

The basis for the method is a transformation which aligns all gage records at zero time, an idea originally suggested by Seamen (Ref. 3). After necessary computation of the required derivatives at a point on the appropriate surface, the results are transformed back into original gage-time using an appropriate fit to the time-of-arrival. In the situations where evaluation of a definite integral along a functional surface is needed, the

integration is calculated as a line integral on the transformed surface.

Differences in interpolation, smoothing, curve and surface fitting, and solution methodology do lead to markedly different results in many cases; the algorithms that were finally chosen are explicitly derived and justified.

While this paper and the subsequent report (Ref. 11), which applies the techniques herein to a specific event, do not address all the possible sources of inconsistency, it will point out many which have not received attention before. Specifically,

1. Errors due to instrumentation inaccuracy.
2. Methodological errors in estimation of strains and stress bounds.

SECTION 2
EQUATIONS OF SPHERICALLY SYMMETRIC FLOW[1]

The equations of motion in the frame tracking a fluid particle (the Lagrangian frame) for spherical 1-D flow are:

$$\frac{\rho_o}{\rho} = \left(\frac{r}{h}\right)^2 \cdot \frac{\partial r(h,t)}{\partial h}\Big)_t \tag{1}$$

$$-\rho(h,t) \cdot \frac{\partial u(h,t)}{\partial t}\Big)_h = \frac{\partial \sigma_r(h,t)}{\partial r}\Big)_t + 2 \cdot \frac{\sigma_r - \sigma_t}{r(h,t)} \tag{2}$$

$$u(h,t) = \frac{\partial r(h,t)}{\partial t}\Big)_h \tag{3}$$

The equations are general for nonisentropic waves[2] and are valid under the following assumptions (Refs. 1 and 12):

1. Heat flow is to be neglected.
2. All body forces are to be neglected.
3. No energy sinks or sources are postulated.
4. All flow is spherical.

Assumptions 1 and 2 are considered valid because of the very short time intervals and high stresses involved. Assumption 3 is generally valid until the point where discontinuous phenomena occur, such as cracking of material or onset of phase changes.

---

1 Equation 1 expresses conservation of mass. Equation 2 expresses conservation of momentum. Equation 3 is the kinematic particle velocity. Note: the convention of Equation 2 is that a tensile stress is negative.

2 A rapidly attenuating shock induced by a detonation on or in the ground being the case of present interest.

Assumption 4 is ideally valid for a perfectly spherical detonation in an isotropic, homogeneous, full space and implies an absence of tangential motions and any shear stresses due to vorticity. Perfectly spherical flow can be interpreted as a singularity at the origin in the equations of motion; i.e., as a mass source, In the case of a contained detonation at large radii, the same idealization applies.

Practically, for detonations in near surface layered media with measurements of unknown absolute accuracy relatively near an expanding crater, the posed problem is really a complex boundary value problem in a nonideal medium. Investigation into disturbing effects resulting from these two considerations and their implications for solution of 1-3 has just begun.

SECTION 3
APPROXIMATION OF FLOW SURFACE

Given an event meeting the assumptions in Section I and a radial stress and motion field approximately described by observed Lagrangian gages, Equations 1-3 can be inverted for the field strains and field stress difference.

In order to do this we consider the spherical one-dimensional flow surface in Figure 1a approximately represented by the observed particle velocity variable[3] (i.e., gage response), u as a function[4] of the coordinates h and t; that is,

$$u = u(h,t).$$

Further

$$u(h_o,t) = \frac{\partial r}{\partial t}\Big)_h \text{ and } r(h_o,t) = h_o + \int_{t_o}^{t} u(h_o,t')dt'. \qquad (4)$$

Define h_o as the initial gage position, and $t_a = f(h)$, as the time-of-arrival of the shock front (ignoring any low level precursor[5]), where f(h) is a fitted function solely of the

---

3 The same procedure applies for measured radial stress.

4 Here we explicitly distinguish between a gage, $u(h_o,t)$, and a flow surface, $u(h,t)$.

5 Elastic precursors occurring in the field at low stresses introduce the problem of being unable to precisely identify f(h) if nothing else is known. The problem is exacerbated if the signal is near the noise floor and/or discrete resolution of the instrumentation. This imprecision turns out to be a potentially important source of error in the low stress regime.

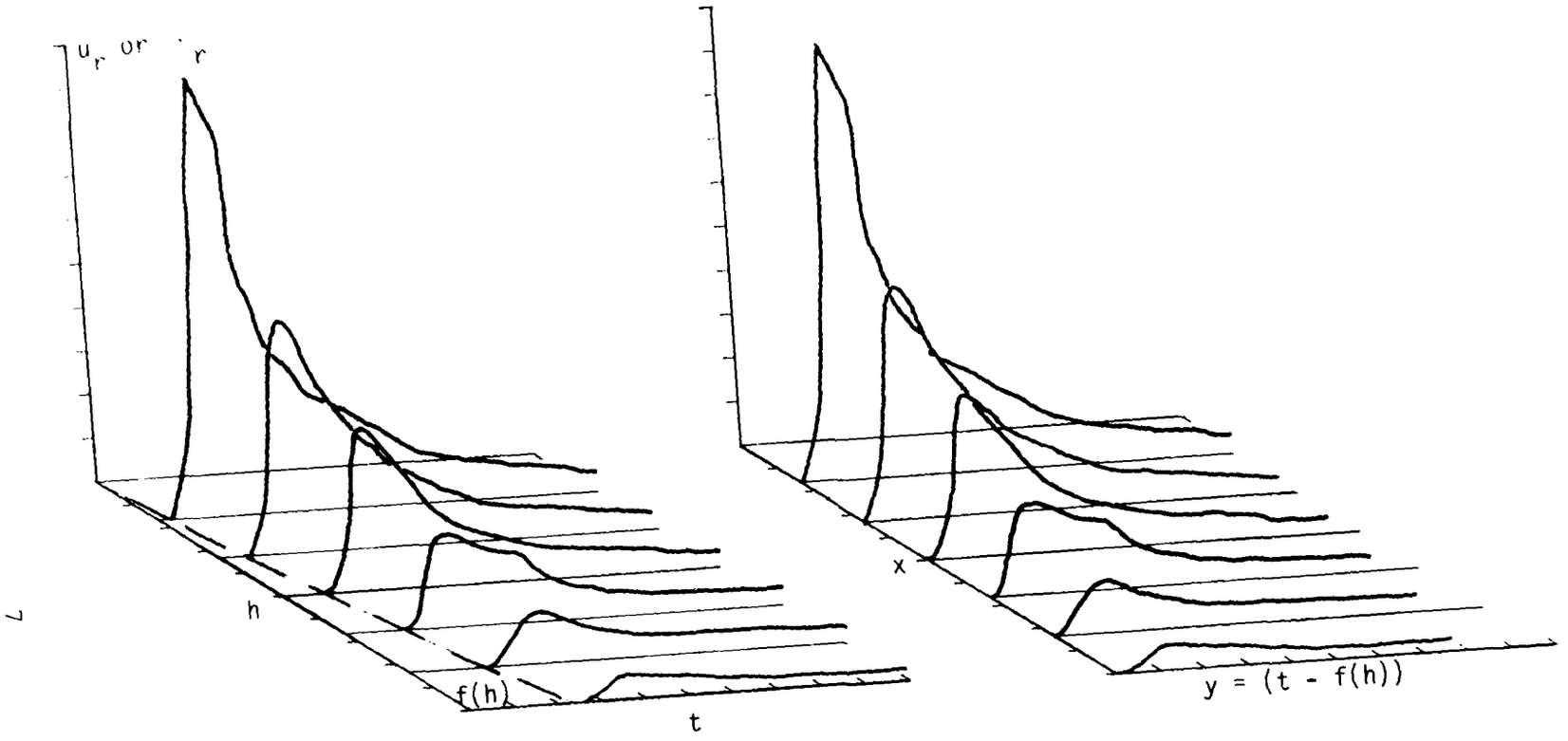

Figure 1a. 1-D stress or velocity flow surface. Untransformed flow surface approximately represented by observed gage responses at discrete values of h.

Figure 1b. Transformed flow surface. Transformed flow surface with f(h) removed. Derivatives at constant t are calculated from functional fits across the flow at y, constant.

Lagrangian gage position; suitable functions will be discussed later.

Contrary to a large body of thought, a complete stress field and motion field and their approximation is not necessary for estimation of the strain path at a point.[6] Indeed, in complex one-dimensional flow, seeking the average stress and motion flow across a large expanse of the field, as measured in several widely spaced locations, is an improper approach since strain is a quantity defined at a point. In practice, what can actually be calculated are relative displacements between discrete gages. One would ideally like to have gages as close as possible (within limits) to the point at which the path is sought in order to have the average calculated strains approach the actual point strains. This is especially true since in geological media it is nearly impossible to establish the regional homogeneity of a material undergoing sharp load-unloading.

We consider the following definition of the new independent variables x and y

$$x = h;$$
$$y = t - t_a = t - f(h) \tag{5}$$

and define the transformation $u(h,t) \rightarrow \mathfrak{U}(x,y)$; the Jacobian, $|J| = -1$, and, thus, if $\mathfrak{U}(x,y)$ is known or approximated, we are certain we can always obtain the global inverse transformation $u(h,t) \leftarrow \mathfrak{U}(x,y)$.

The transformation $u(h,t) \rightarrow \mathfrak{U}(x,y)$ has the practical effect of aligning the characteristic lines of (generally) inhomogeneous

---

6 It is, however, a necessity for calculation of stress bounds and is helpful in gage validation efforts.

flow so that they all begin at (x,0) (see Fig. 1b). Exterior derivatives across the lines of flow in {x,y} can then be much more accurately approximated than is possible in {h,t}.

We note the following identity

$$u(h,t) \equiv \mathfrak{U}[h,t - f(h)]. \tag{6}$$

The transformation (Eqn. 6) introduces no inherent error. However, it does presume that f(h) is accurately known. This is equivalent to the presumption that the initial gage locations are accurately known and that the gage timing is correct.

SECTION 4
APPROXIMATING THE TRANSFORMED FLOW SURFACE AT X,Y

The transformed surface may be approximated at a point x_o, y_o as

$$\tilde{u}(x,y)|_{x_o,y_o} = \tilde{u}_1(x,y_o) + \tilde{u}_2(x_o,y) - u(x_o,y_o) \tag{7}$$

and globally as piecewise continuous polynomials. The approximation is thus a numerical surface described by orthogonal splines.

In particular, we choose u_1 and u_2, quadratic in y and quadratic in x, as

$$\tilde{u}_1(x,y_o) = a_o + a_1 x + a_2 x^2, \tag{8}$$

$$\tilde{u}_2(x_o,y) = b_o + b_1 y + b_2 y^2. \tag{9}$$

We also wish to consider $\tilde{u}_1$ quadratic in ln(x) or

$$\ln(\tilde{u}_1(x,y_o)) = a_o + a_1 \ln(x) + a_2 \ln^2(x) \tag{10}$$

in order to more accurately approximate a flow surface that attenuates very steeply with increasing range.

The function $u_1(x,y_o)$ is approximated by the observed transformed values at three gages at a constant, transformed time, y_o. Generally, the number of gages available at distinct ranges is limited; we assume here that three gage records are available, an "inner" and "outer" gage and a center gage at the range of interest. Thus, the approximating quadratic is

perfectly determined and is given by an augmented Vandermonde determinant

$$\det \begin{pmatrix} \tilde{u}_1(x,y_o) & 1 & x & x^2 \\ \tilde{u}_1(x_{m-1},y_o) & 1 & x_{m-1} & x_{m-1}^2 \\ \tilde{u}_1(x_m,y_o) & 1 & x_m & x_m^2 \\ \tilde{u}_1(x_{m+1},y_o) & 1 & x_{m+1} & x_{m+1}^2 \end{pmatrix} = 0, \qquad (11)$$

with a similar expression holding for $\ln(u_1)$. An example of such a fit is shown in Figure 2.

The situation of finding the three constants, b_o, b_1, and b_2, which are used to approximate the velocity along the flow must be approached by a different route. The accuracy of locally approximated derivatives along a velocity gage can be severely affected by initial sampling rate, resampling rate, noise and record band-width, and unexplainable jerks and jumps. (It will turn out that a discontinuity in velocity (leading to an impulse in acceleration) will be integrated, leading to a unit-step discontinuity in calculated strains unless smoothed over.) The result is that while a low order least-squares polynomial spline is used to locally approximate the spline u_2, the fit must be made carefully in the sense that velocity and displacement recomputed from the approximated acceleration record must be shown to be consistent. Both linear and quadratic splines were tried.

Figure 3a shows an accelerometer response for an event with its integrated velocity record. The estimated acceleration using the velocity record for two different trials is shown in Figure 3b. The sampling rate was 10 μsec per point, which insured

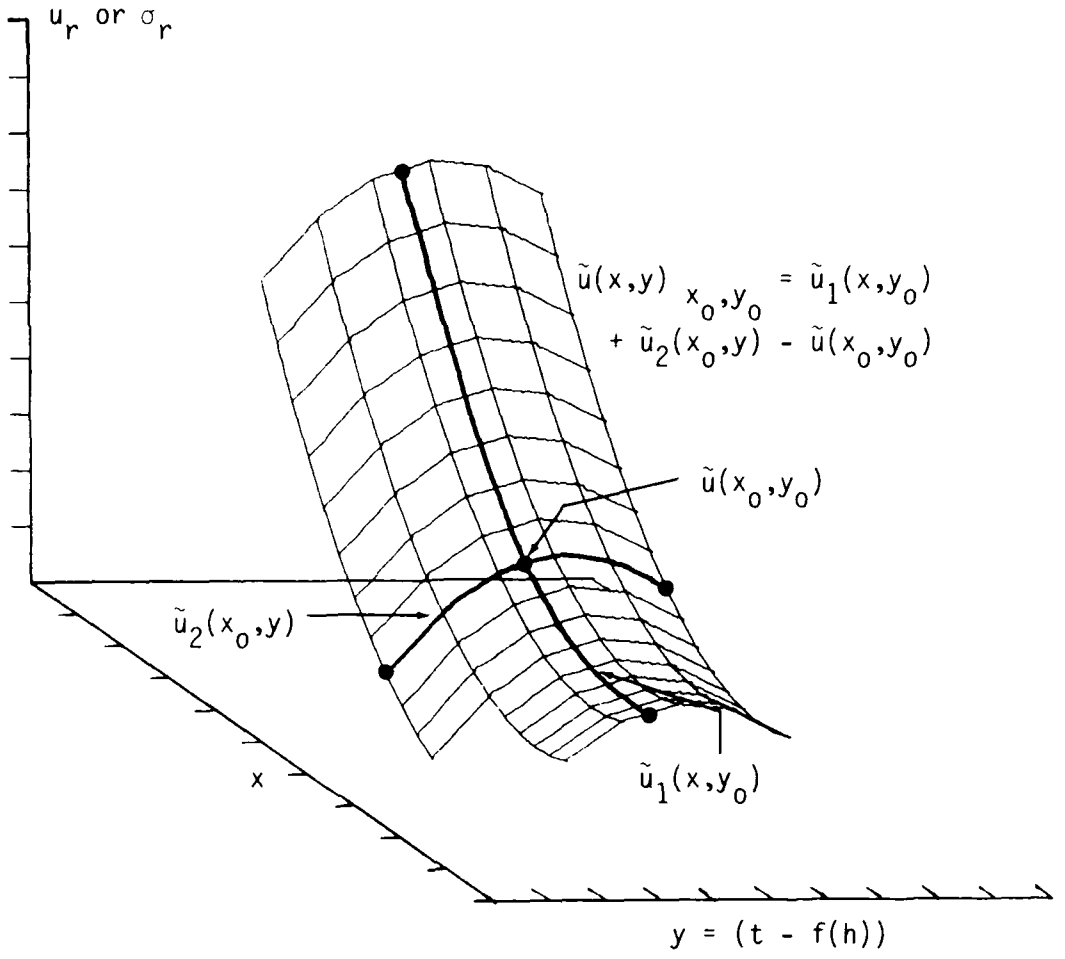

Figure 2. Orthogonal splines on the transformed surface used for calculating the required partial derivatives in the neighborhood of the point, $\tilde{u}(x_o,y_o)$. The splines are approximated in different ways.

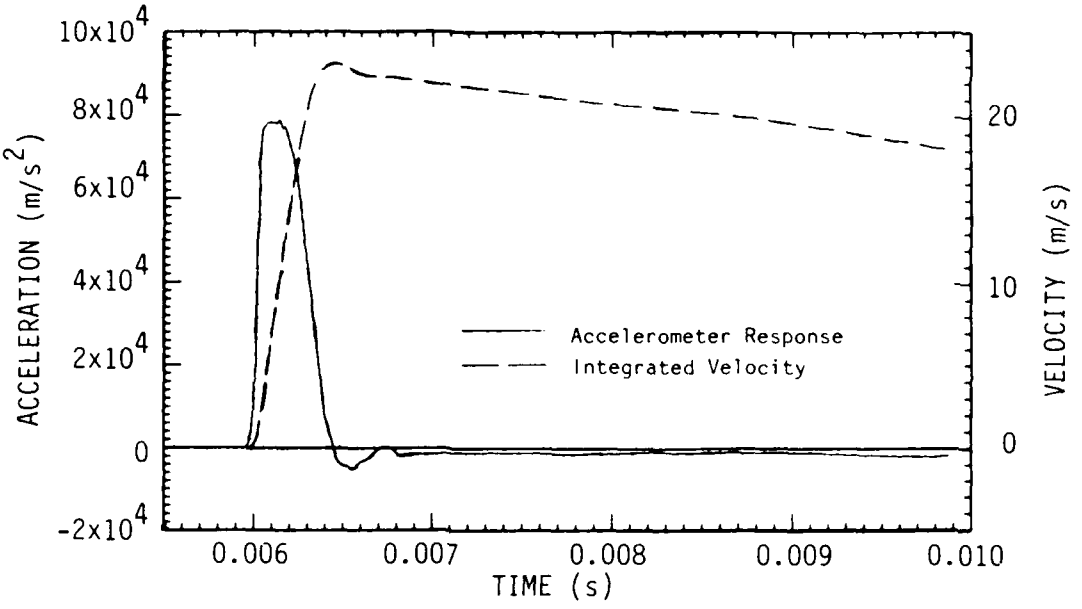

Figure 3a. Measured acceleration in recompacted dry alluvium.

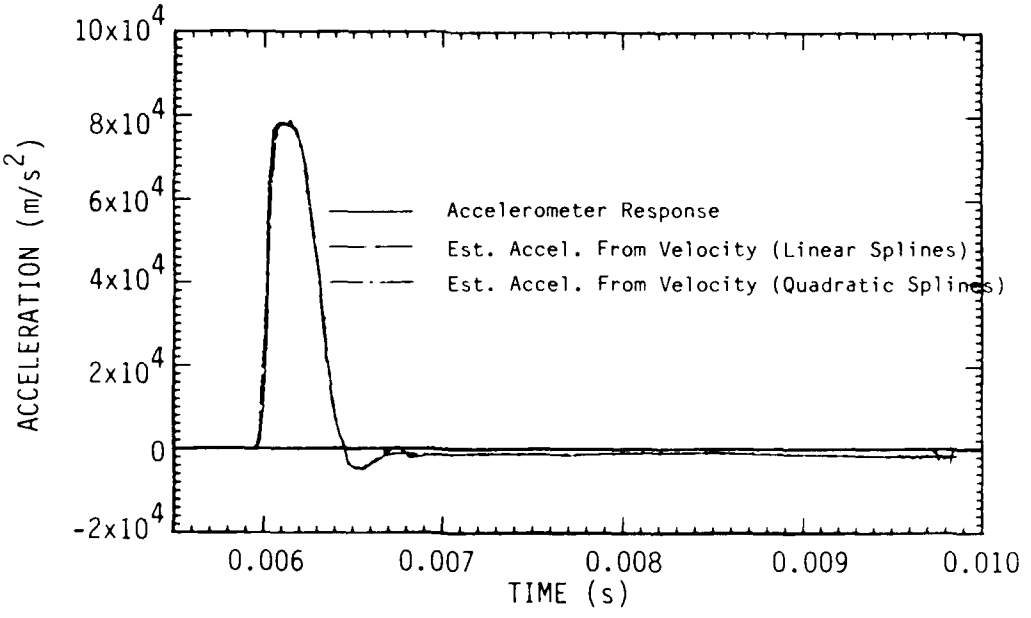

Figure 3b. Measured acceleration in recompacted dry alluvium compared to two estimates from velocity.

adequate resolution of the peak. Trial 1 used a linear spline with a moving window of 20% time-to-peak until peak and a larger window (by a factor of 4) during decay. Trial 2 used a quadratic spline, again with a moving window of 20% time-to-peak; the window during decay was multiplied by a factor of 10 in this case.

Both fits are nearly identical except for the error in Trial 1 introduced by the linear spline averaging across the rather small rise in velocity immediately after peak. The quadratic spline in Trial 2 is a nearly perfect estimate of the original accelerometer. No filtering was done to the velocity record or the estimated accelerations in this case. Both splines appear to be adequate. Experience has shown, however, that:

1. Equivalent accuracy with a linear spline requires smaller windows and higher sampling rates than for a quadratic spline.

2. A larger window during decay is needed when using a quadratic spline than with a linear spline; this is especially true with decays exhibiting an 'oscillatory' character. An insufficiently windowed quadratic spline has the nasty tendency to capture regions of inflection. This leads to extremely high and unrealistic impulses in estimated acceleration.

3. Extremely noisy velocity records mandate a linear spline (or some degree of filtering, see below).

Ideally, some type of smoothing should be done to allow small fitting windows to be used so that the detailed structure of the velocity waveform is captured (not attributable to stochastic processes). A finite impulse response (FIR) low pass

filter with linear phase characteristics that is useful is an n-repeated three point moving average filter (Ref. 13);

$$u_j \leftarrow \frac{1}{3}(u_{j-1} + u_j + u_{j+1}). \tag{12}$$

The filter usually only needs to be applied after rise-to-peak;[7] the number of applications to a record depends on the initial band width and power spectra. This filter is especially useful for effectively filtering calculational records, which generally s[Aw clear trends despite the presence of numerical oscillations about the trend.

The untransformed derivatives for the approximating splines u_1 and u_2 given by Equations 8 and 10 are derived next. The starting point is the earlier recognition that $u(h,t) \equiv u[h,t - f(h)]$. Thus, the spatial and temporal derivatives are, in terms of x and y,

$$\left.\frac{\partial u(h,t)}{\partial h}\right)_t = \left.\frac{\partial \tilde{u}[h,t - f(h)]}{\partial h}\right)_t$$

$$\text{and} \quad \left.\frac{\partial u(h,t)}{\partial t}\right)_h = \left.\frac{\partial \tilde{u}[h,t - f(h)]}{\partial t}\right)_h \tag{13}$$

where t - f(h) is being treated as a new independent variable, say z. Using the chain rule,

---

[7] The reason being that early-time accelerations are very high and easily approximated with sufficient sampling of the velocity waveform. Accelerations after peak velocity can easily be several orders of magnitude smaller than the initial accelerations. (See Fig. 3a.)

$$\left.\frac{\partial u(h,t)}{\partial h}\right)_t = \left.\frac{\partial \tilde{u}(x,z)}{\partial h}\right)_t = \left.\frac{\partial \tilde{u}}{\partial x}\right)_z \cdot \left.\frac{\partial x}{\partial h}\right)_t + \left.\frac{\partial \tilde{u}}{\partial z}\right)_y \cdot \left.\frac{\partial z}{\partial h}\right)_t \qquad (14)$$

which reduces to

$$\left.\frac{\partial u(h,t)}{\partial h}\right)_t = \left.\frac{\partial \tilde{u}}{\partial x}\right)_z \cdot 1 - \left.\frac{\partial \tilde{u}}{\partial z}\right)_y \cdot f_h(h). \qquad (15)$$

In problems like this it is often helpful to explicitly indicate which independent variable(s) is (are) being treated as constant.

The approximating surface in {x,y} is given by

$$\tilde{u}(x,y) = e^{a_o} x^{a_1 + a_2 \ln(x)} + b_o + b_1 y + b_2 y^2 - \tilde{u}(x_o, y_o). \qquad (16)$$

Therefore,

$$u(h,t) = \tilde{u}(x,z) =$$

$$e^{a_o} x^{a_1 + a_2 \ln(x)} + b_o + b_1 z + b_2 z^2 - \tilde{u}(x_o, y_o). \qquad (17)$$

Hence,

$$\left.\frac{\partial \tilde{u}(x,z)}{\partial x}\right)_z = e^{a_o} [a_1 + 2a_2 \ln(x)] x^{a_1 - 1 + a_2 \ln(x)}, \text{ and,} \qquad (18)$$

$$\left.\frac{\partial \tilde{u}(x,z)}{\partial z}\right)_y = b_1 + 2b_2 z. \qquad (19)$$

And finally, substituting these derivatives into Equation 15:

$$\left.\frac{\partial u(h,t)}{\partial h}\right)_t = e^{a_o}[a_1 + 2a_2\ln(h)]h^{a_1-1+a_2\ln(h)} - f_h(h)[b_1 + 2b_2(t - f(h))]. \quad (20)$$

To evaluate the acceleration in {h,t} we again use Equation 13

$$\left.\frac{\partial u(h,t)}{\partial t}\right)_h = \left.\frac{\partial \tilde{u}(x,z)}{\partial t}\right)_h = \left.\frac{\partial \tilde{u}}{\partial x}\right)_z \cdot \left.\frac{\partial x}{\partial t}\right)_h + \left.\frac{\partial \tilde{u}}{\partial z}\right)_y \cdot \left.\frac{\partial z}{\partial t}\right)_h. \quad (21)$$

This reduces to

$$\left.\frac{\partial \tilde{u}(h,t)}{\partial t}\right)_h = b_1 + 2b_2[t - f(h)]. \quad (22)$$

And, of course, acceleration is seen to be invariant whether it is approximated in {x,y} or {h,t}.

Important to note is that the preceding approximations are not global; they are valid only in the region $\{x_o,y_o\}$. Therefore, while the approximating function may be legitimately differentiated at x_o,y_o, integration outside the immediate neighborhood of the point is not permissible.

Nothing has been said of the form of f(h) or means for its approximation. Three different functional forms found useful are

$$
\begin{aligned}
t_a = f(h) &= a_o + a_1 h \\
&= a_o + a_1 h + a_2 h^2 \\
&= e^{a_o} h^{a_1 + a_2 \ln(h)} \quad .
\end{aligned}
\tag{23}
$$

Selection and fitting of a form of f(h) can be done in two ways. In one approach, various forms can be fitted to all data points. Then the form which minimizes error according to any of several criteria is used. The second approach is to fit f(h) locally, using data points in the neighborhood of the differencing gage location.

The most appropriate approach is problematical. On the one hand, if gage time-of-arrivals (or, especially, surveyed gage positions) are highly suspect, the only possible approach would appear to be to estimate f(h) in the neighborhood by a fit to all available data points. On the other hand, if gage positions and time-of-arrivals are known to be accurate, approximation of f(h) should be done in the neighborhood of h_o.

SECTION 5
APPROXIMATING STRAIN-TIME HISTORIES

We start with the following definitions of strain in one-dimensional spherical flow:[8]

$$\epsilon_t = 1 - \left(\frac{r}{h}\right) \qquad \epsilon_r = 1 - \frac{\partial r(h,t)}{\partial h}$$

$$\epsilon_v = 1 - \left(\frac{r}{h}\right)^2 \cdot \frac{\partial r(h,t)}{\partial h} \tag{24}$$

Note that ϵ_v is the full strain of a unit volume element with principal axes, χ_r, χ_θ, χ_t, undergoing extensional strains of $-\epsilon_r$ and $-\epsilon_t = \epsilon_\theta$. That is,

$$\epsilon_v = 1 - \prod_{i=1}^{3} (1 + \epsilon_i)$$

In order to explicitly evaluate the above strains in terms of the approximate surface, we begin with the Eulerian position expressed in terms of the Lagrangian gage position and the gage response as a function of Lagrangian position and time.

Using Equation 4, we can write the strains as:

$$\epsilon_t(h_o,t) = -\frac{1}{h_o} \cdot \int_{f(h_o)}^{t} u(h_o,t)dt,$$

$$\epsilon_r(h_o,t) = -\int_{f(h_o)}^{t} \frac{\partial u(h,t)}{\partial h}dt, \tag{25}$$

---

8 A strain which produces compression is positive in this text.

$$\epsilon_v(h_o,t) = 1 - \left(\frac{r}{h}\right)^2 \cdot \left[1 + \int_{f(h_o)}^{t} \frac{\partial u(h,t)}{\partial h} dt\right].$$

Other commonly employed variables, μ and ρ are found from ϵ_v by the following formulas:

$$\mu = \frac{\epsilon_v}{1 - \epsilon_v} \text{ and } \rho = \frac{\rho_o}{1 - \epsilon_v} \quad . \tag{26}$$

Generally, the number of long-term surviving gages providing acceptable velocity-time histories is small enough that a global fit to the entire flow surface is an ill-defined undertaking. Practically, Equations 25 are best evaluated in discrete time-steps with a local approximating surface, u(h,t) found for each time-step.

The technique resulting from this paper assumes at least three gages[9] are available and uses the approximating polynomials from the previous section to calculate the spatial and time derivatives at each time-step. The defining equations for strains are integrated over each time-step and the terms cumulatively summed. A typical term using a quadratic polynomial (Eq. 8) fit across the flow (h direction) and a quadratic fit (Eq. 9) along the flow (acceleration as a function of time) is:

$$\int_{f(h_o)+k\Delta t}^{f(h_o)+(k+1)\Delta t} \frac{\partial \tilde{u}[h,t - f(h)]}{\partial h}\Bigg|_{(k)} dt = \Delta t\left[a_1^{(k)} + 2h_o a_2^{(k)} - b_1^{(k)}\right.$$

---

9 Use of a larger number of gages to approximate the a_i's is certainly possible and, in some cases (i.e., if the strain field is known a priori to be exceptionally uniform), probably preferable. However, as mentioned before, there are definite reasons why a field-wide fit should not be done.

$$\cdot f_h(h_o)\Big] - \Delta^2 t \cdot (2k+1) \cdot f_h(h_o) \cdot b_2^{(k)}, \qquad (27)$$

where each of the a_i and the b_i is approximated at $f(h_o) + k\Delta t$ as indicated previously. The second order term is a result of the quadratic fit to the velocity and cannot be neglected. Also, note that the limits of integration are evaluated at a specific gage, h_o, and are considered constant for each integration.

Thus, for example, a numerical solution to Equation 25 (ϵ_r) is derived in full

$$\epsilon_r(h_o,t) = -\sum_{k=0}^{k_{max}} \left[\Delta t\left(a_1^{(k)} + 2h_o a_2^{(k)} - b_1^{(k)} \cdot f_h(h_o)\right)\right.$$

$$\left. - \Delta^2 t \cdot (2k+1) \cdot f_h(h_o) \cdot b_2^{(k)}\right]. \qquad (28)$$

If Equation 10 is used to approximate the flow across the gages instead of 8, the solution is

$$\epsilon_r(h_o,t) = -\sum_{k=0}^{k_{max}} \left[\Delta t\left(e^{a_o^{(k)}}\left[a_1^{(k)} + 2a_2^{(k)}\ln(h_o)\right]\right.\right.$$

$$\left. \cdot h_o^{a_1^{(k)}-1+a_2^{(k)}\ln(h_o)} - b_1^{(k)} \cdot f_h(h_o)\right)$$

$$\left. - \Delta^2 t \cdot (2k+1) \cdot f_h(h_o) \cdot b_2^{(k)}\right] \qquad (29)$$

where k_{max} corresponds to the index of the final time-point. The

ratio, $\left(\frac{r}{h}\right)^2$ in Equation 24 is equal to:

$$\left[1 + \frac{1}{h_o} \cdot \int_{f(h_o)}^{t} u(h_o,t)dt\right] \tag{30}$$

where the integral must be evaluated numerically. Note that the integral is simply a displacement history along a gage (h constant) and may be evaluated by several well known schemes.

SECTION 6
CALCULATION OF STRESS DIFFERENCE FROM COMBINED VELOCITY/STRESS RECORDS

The conservation of momentum equation can be solved for the stress difference as follows:

$$\kappa(h_o,t) = \sigma_r - \sigma_t =$$

$$-\frac{r}{2}\left[\left(\frac{\rho_o}{1+\epsilon_v} \cdot \frac{\partial u}{\partial t}\right)_{h_o}\right] - \left[\left(\frac{1}{1+\epsilon_r} \cdot \frac{\partial \sigma_r}{\partial h}\right)_{h_o}\right] \qquad (31)$$

The spatial derivative of radial stress can be approximated in the same manner as was done for velocity; the indicated strains are presumably already at hand. Thus, with three velocity records and three stress records, the stress difference at the location of the center gage can be found. The location of the center stress and velocity gage must coincide. If they do not, interpolation across the gages[10] can be done to provide a "gage."

Calculation of κ hinges on accurate determination of $\mathring{u}(h_o,t)$, and use of the splines and filtering methods of Section 4 will do a lot to reduce a noisy result to a clear stress path. In practice, estimation of $\mathring{u}$ will be the limiting factor in estimating κ.

Note that, to first order, the stress difference is in error directly proportional to the error in displacement due to the term, $r(h,t)$.

---

10 See Section 4.

SECTION 7
STRESS BOUNDS

Trulio's (Ref. 6) lower stress bound equation can be obtained directly from the equation of momentum conservation by assuming the media is a perfect fluid and, hence, the stress difference is identically equal to zero. Then integrating along a path of constant, t,

$$-\rho(h,t) \cdot \frac{\partial u(h,t)}{\partial t}\Big)_h = \frac{\partial \sigma_r(h,t)}{r}\Big)_t$$

$$\rightarrow \quad \sigma_r^L(h,t) = \int_{r_g(t)}^{r_f(t)=t\cdot c_s} \rho \dot{u} dr \tag{32}$$

Figure 4 is given as an aid in visualizing the paths of integration in this integral and the one that follows.

The corresponding Lagrangian integral is found by observing that the total differential, dr, is

$$dr = \frac{\partial r}{\partial h}\Big)_t dh + \frac{\partial r}{\partial t}\Big)_h dt \tag{33}$$

and along a path of constant time:

$$\sigma_r^L(h_g,t) = \int_{r_g(t)}^{r_f(t)=t\cdot c_s} \rho \dot{u} dr = \rho_o \cdot \int_{h_g}^{h_f(t)} \left(\frac{h}{r}\right)^2 \dot{u} dh \tag{34}$$

where the final integral in Lagrangian coordinates is found by applying conservation of mass (Eq. 1) to eliminate $\partial r/\partial h$. Note

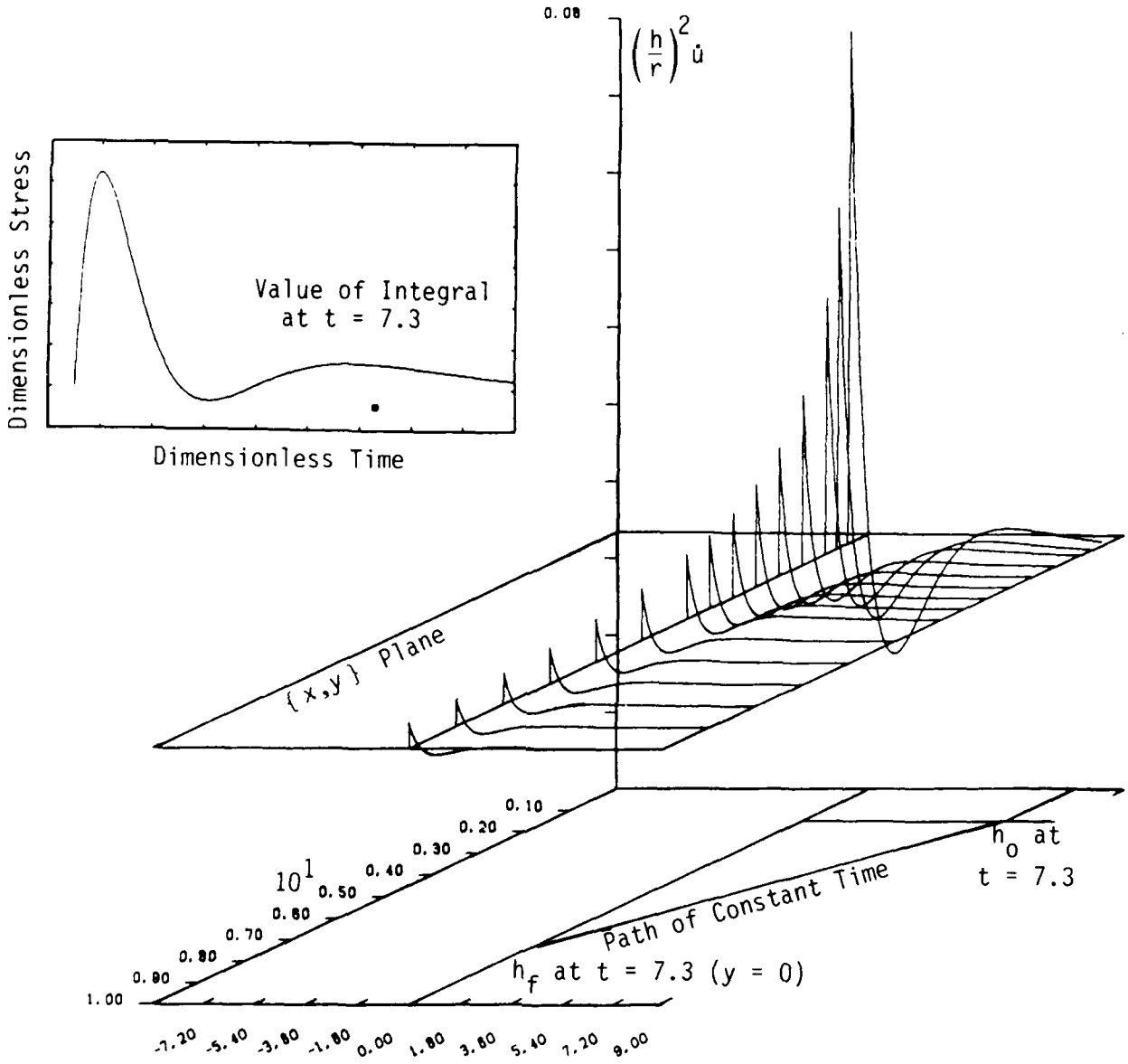

Figure 4. Surface of lower stress bound integrand using spherical cavity test problem. The lower stress bound integral is given by the area under the displayed surface along a path of constant time projected onto the (x,y) plane, beginning at h_0 and ending at h_f. h_f is a function of time, making the stress bound a function of h_0 and time. Below, the path of constant time (a linear function in the test problem) is shown, along with the gage line, h_0, at a range of 1.5 and time of 7.3, and the upper limit of the integral at h_f. Note that h_f is at the advancing wave front at y = 0; further integration along the path would contribute nothing to the integral. Note that integration at ranges where h_f exceeds the measured field (h = 10, here), the stress bound requires extrapolation. The possible error is not always small.

that the upper limits of integration are identical since r = h at the advancing wave front.

Under the assumption that tangential stresses can never exceed the material tensile limit, θ, an upper bound to radial stress, can be found, viz.:

$$\sigma_r^U(h_g,t) = \theta\left[\left(\frac{r_f}{r_g}\right)^2 - 1\right] + \rho_o \cdot \int_{h_g}^{h_f(t)} \left(\frac{h}{r_g}\right)^2 \dot{u}dh \qquad (35)$$

Evaluation of Equations 34 and 35, which are line integrals over the transformed surface (that is, the path of integration is not along either of the transformed axis), is somewhat subtler than the estimation of strains, which merely requires approximation of the local function surface at a point.

Some difficulty is also introduced in the following way: the functional surfaces used in the strain relations are those of velocity and displacement, surfaces which tend to be smooth (especially the displacement surface), and numerically predictable.

The two surfaces described by the integrands of the stress bound formula are rather complex, being functions of both acceleration and reciprocal displacement. We have found the following numerical technique to give answers which match well with known results.

The profiles of the transformed surface to be approximated are calculated per the methods of Section II. A global approximation to the surface is then constructed using the following basis functions (Refs. 14, 15,and 16):

1. Linear polynomials in y.
2. Cubic splines in x.

SECTION 8
TEST PROBLEMS FOR SOLUTION METHODS

Several different numerical solutions of the equations of spherical flow in soils and rocks have been reported (Refs. 1, 3, and 4). Generally, the methods have first been applied to waveforms from problems with known solutions in order to obtain an idea of the errors and difficulties associated with each numerical method. This is done here.

The following analytic problem is adapted in large part from Grady, (Ref. 1), and was used to ascertain the accuracy of our solution procedure. In addition, the method is applied to ascertain the accuracy of the solution method used in computing the stress bounds introduced by Trulio. In addition, stress and velocity waveforms from a 1-D spherical calculation, simulating a contained nuclear detonation (yield = 15.15 kt) in Yuma alluvium were used as more representative of the input for which the method was developed.

Consider an expanding cavity (with prescribed elastic boundary conditions) in an infinite homogeneous isotropic medium. The field solution can be written in terms of a scalar elastic potential; for waves moving away from the cavity the solution in terms of dimensionless length (H) and time (T) is

$$\psi = \frac{1}{H} \cdot f(H - T);$$

$$U = \frac{\partial \psi}{\partial H} \qquad (36)$$

where U is the displacement as seen by a fixed observer in an inertial (Eulerian) frame. We choose ν = 0.25, K = 5/9 and G = 1/3, and the dimensionless rest density and elastic sound speed will equal unity. The boundary conditons are

Displacement at cavity: $U(1,T) = g(1 - T)$, $T > 1$,

Displacement vanishes at wave front: $U(T,T) = 0$, $T > 1$.

Let $\varsigma = H - T$. The solution in terms of the cavity displacement is:

$$f(\varsigma) = e^{\varsigma} \int_{o}^{\varsigma} e^{\varsigma'} g(\varsigma') d\varsigma' \tag{37}$$

All field quantities of interest can be calculated in terms of $f(\varsigma)$,

$$U = -H^{-2} f + H^{-1} f'$$

$$V = H^{-2} f' - H^{-1} f''$$

$$A = -H^{-2} f'' + H^{-1} f'''$$

$$\epsilon_v = -H^{-1} f''$$

$$\epsilon_r = -H^{-1} f'' + 2H^{-2} f' - 2H^{-3} f \tag{38}$$

$$\epsilon_t = -H^{-2} f' + H^{-3} f$$

$$\sigma_r = (1 - \nu)^{-1} \cdot \left[(1 - \nu) \frac{f''}{H} - (1 - 2\nu) \left(\frac{f'}{H^2} - \frac{f}{H^3} \right) \right]$$

$$\sigma_t = (1 - \nu)^{-1} \cdot \left[\nu \frac{f''}{H} + (1 - 2\nu) \left(\frac{f'}{H^2} - \frac{f}{H^3} \right) \right]$$

If we describe the same test problem as Grady, $g(\varsigma) = 0.02\varsigma^2 e^{\varsigma}$, $\varsigma < 0$, then

$$
\begin{aligned}
f &= 0.00667\varsigma^3 e^{\varsigma}, \\
f' &= \varsigma^2 e^{\varsigma}(0.02 + 0.00667\varsigma), \\
f'' &= \varsigma e^{\varsigma}(0.00667\varsigma^2 + 0.04\varsigma + 0.04), \\
\text{and } f''' &= \varsigma e^{\varsigma}(0.00667\varsigma^2 + 0.06\varsigma + 0.12 + 0.04\varsigma^{-1}).
\end{aligned} \tag{39}
$$

Figure 5 is the results of the method applied to the problem of estimating the strains at H = 6, using the known velocity waveforms at H = 5, 6, 7 (Eq. 38). At a sufficiently high sampling rate, the difference between the known strains and the estimated strains is very small.

The upper and lower stress bounds, in terms of the test problem, are:

$$
\sigma_r^L(H_g,T) = \int_{H_g}^{H_f(T)=T} A \cdot \left(\frac{H}{R}\right)^2 dH = \int_{H_g}^{H_f(T)=T} \frac{A\,dH}{\left(1 + \frac{U}{H}\right)^2}
$$

$$
\simeq \int_{H_g}^{H_f(T)=T} A\left[1 - 2\left(\frac{U}{H}\right)\right] dH \tag{40}
$$

$$
\sigma_r^U(H_g,t) = \theta\left[\left(\frac{T}{H_g + U_g}\right)^2 - 1\right] + \frac{\rho_o}{H_g + U_g} \cdot \int_{H_g}^{H_f(T)} AH^2 dH \tag{41}
$$

where the final integral for the lower bound is an approximation derived by assuming U << H. This is generally a valid assumption at moderate to distant ranges and early to moderate times. The integrals are evaluated numerically.

Results of the method for estimating stress bounds discussed in Section VI, compared to known upper and lower solutions calculated at H = 5 from Equations 40 and 41, are shown in Figure

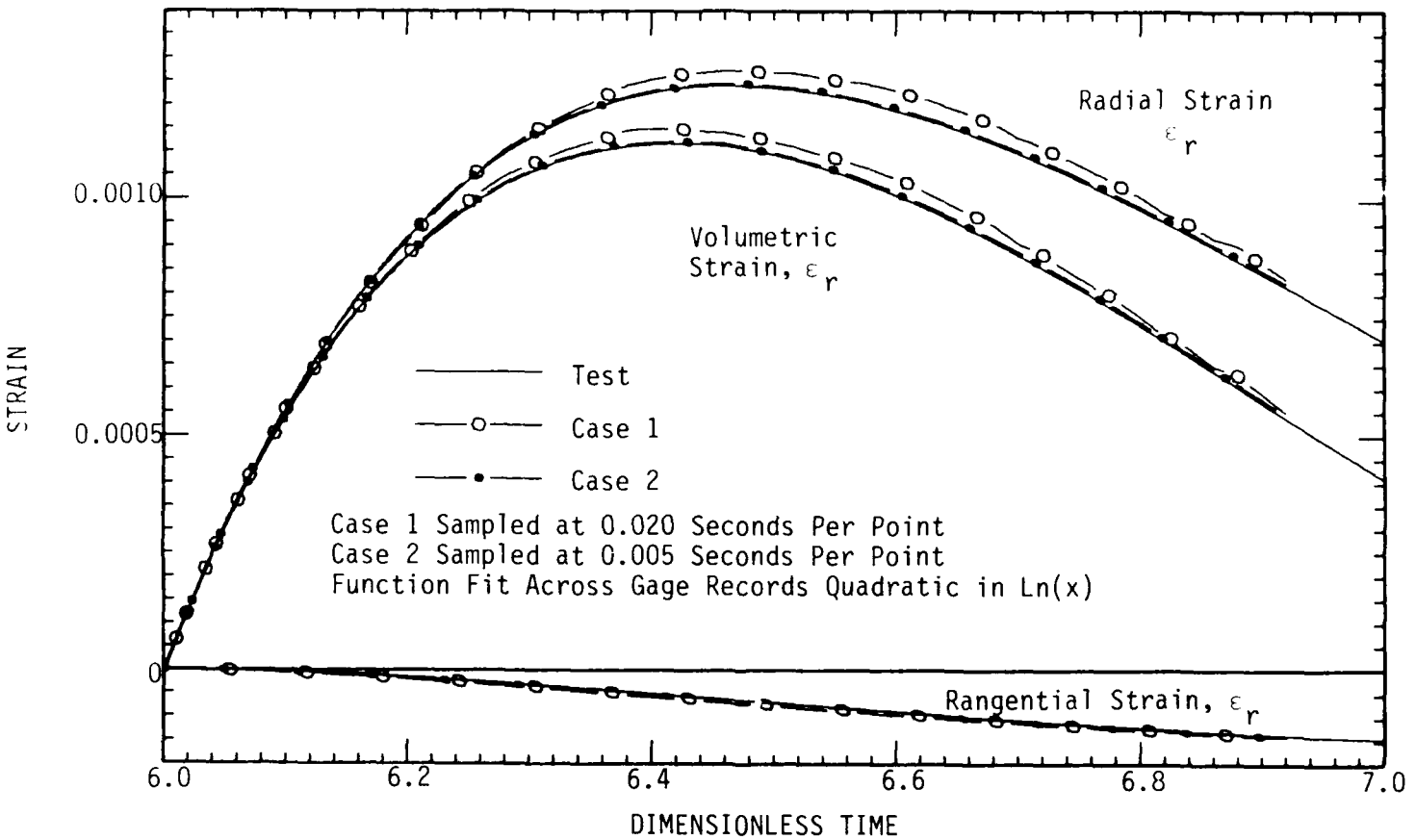

Figure 5. Comparison of Lagrangian strain estimation with analytical spherical cavity test problem.

6a. Surface profiles were calculated at H = 6, 7, 8. The tensile limit was zero in Equation 41. The late-time match is very good. This is to be expected, as the length of the integration interval grows and encompasses more profiles. Error at early time is to be expected for two reasons:

1. The known accelerations in the test problem have a finite value at t_{0+}.
2. The step size is necessarily finite.

However, the errors are quite small.

Figure 6b shows the magnitude of the integrands at three times--early, moderate, and late, as a function of H. This plot provides some indication of where the largest errors might be expected to occur.

Note that, at late times, increasingly large contributions arise from the accelerations occurring at the surface close to H_f. In practical terms, the late-time stress bounds must include an error due to any indeterminancy in measuring velocity rise times. That is, rise times that are too long will give a falsely lower bound.

A one-dimensional finite difference calculation was run in order to provide a test loading more comparable (in both stress and material) to loadings of current interest.

Pertinent information about the calculations:

1. Material: Yuma alluvium, 14-16% air filled voids, ρ_o = 1.89 gm/cc
2. Zone size: 0.2 meters
3. Yield: 15.15 kt

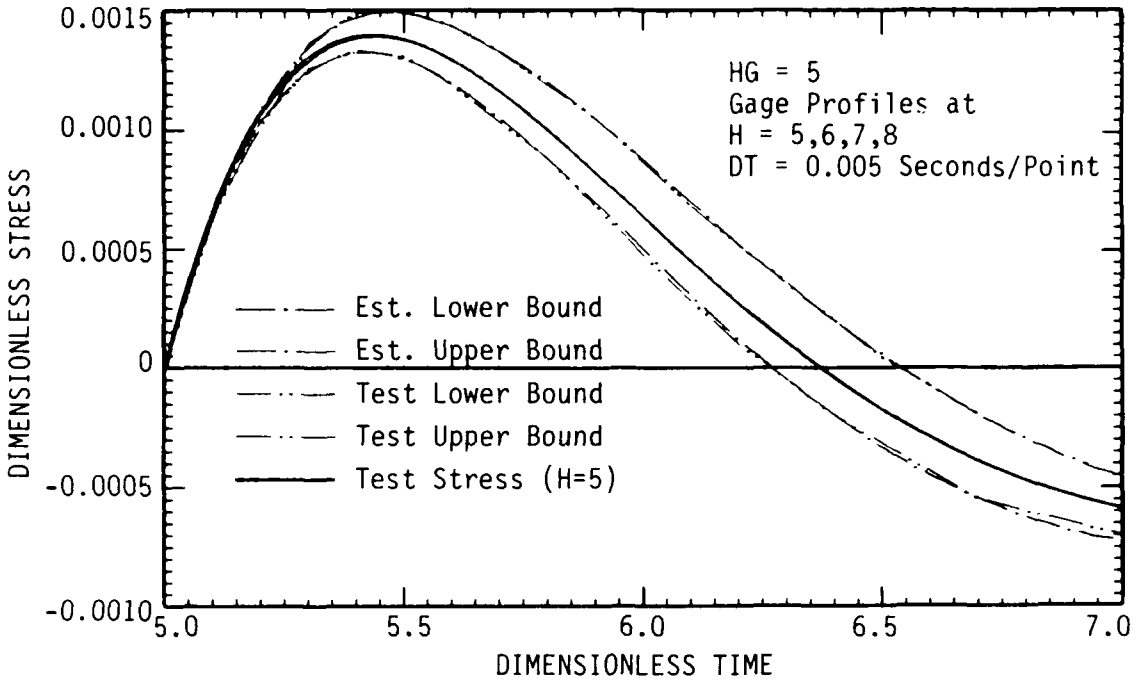

Figure 6a. Comparison of estimated stress bounds with analytical spherical cavity test problem.

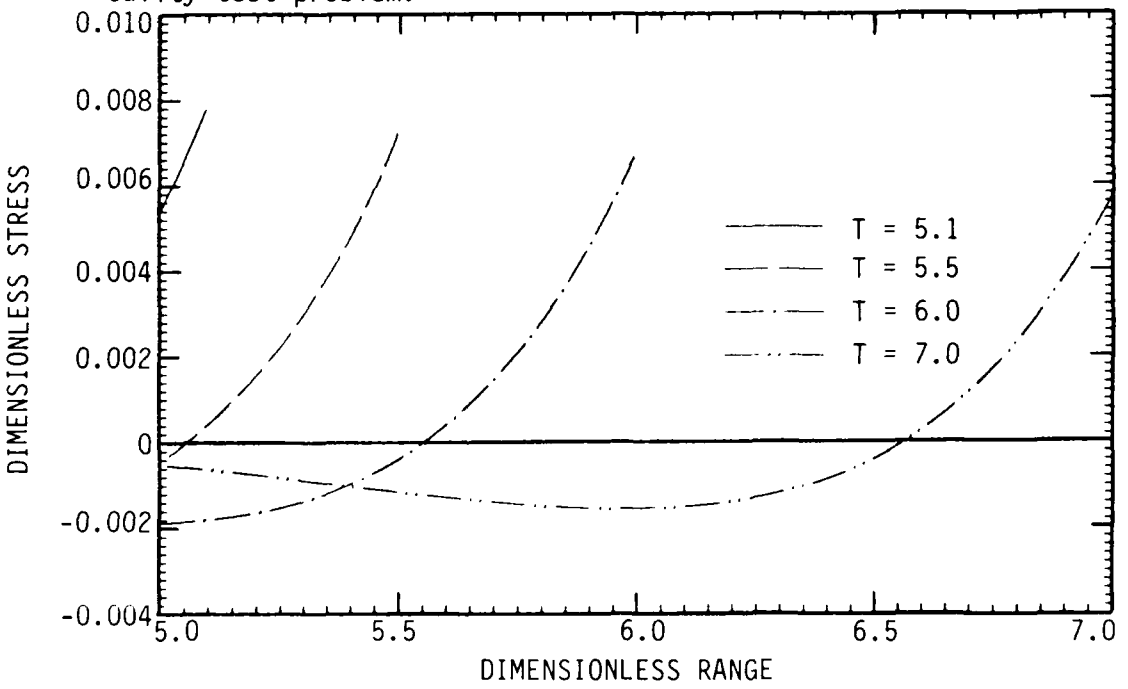

Figure 6b. Magnitude of lower stress bound integrand spherical 1-D test problem (at four times).

4. Point of interest (center point): 20 meters
5. Peak velocity at POI: Approximately 650 m/sec
6. Peak radial stress at POI: Approximately 30 kbar

Figure 7 shows the stress and velocity-time histories from the calculation.

Figure 8 shows the estimated radial and volumetric strains compared against the known strains from the calculation.

The estimated strains initially appear to match well with the known strains though with decreasing accuracy as the width of the estimation interval increases.

Considering Trial 3 to be grossly in error, we would predict that, to first order, estimation intervals in this media at these initial loading conditions should be limited to the interval in Trial 2:

$$\frac{24 - 16 \text{ (m)}}{15.15 \text{ kt}^{1/3}} = 6.0 \text{ m/kt}^{1/3} \qquad \text{(fully contained)}$$

The effect of the error in Trial 1, while seemingly small at the scale shown, is actually enormous, when considered at the scale that would be required for estimation of the material model.

Figure 9 shows the known strain paths in the calculation at 20 meters compared with the strain path obtained from the Lagrangian analysis, the stress used being the calculated stress and, thus, not subject to validation. The estimated model is clearly diametrically opposite in all respects to the model that was actually used.

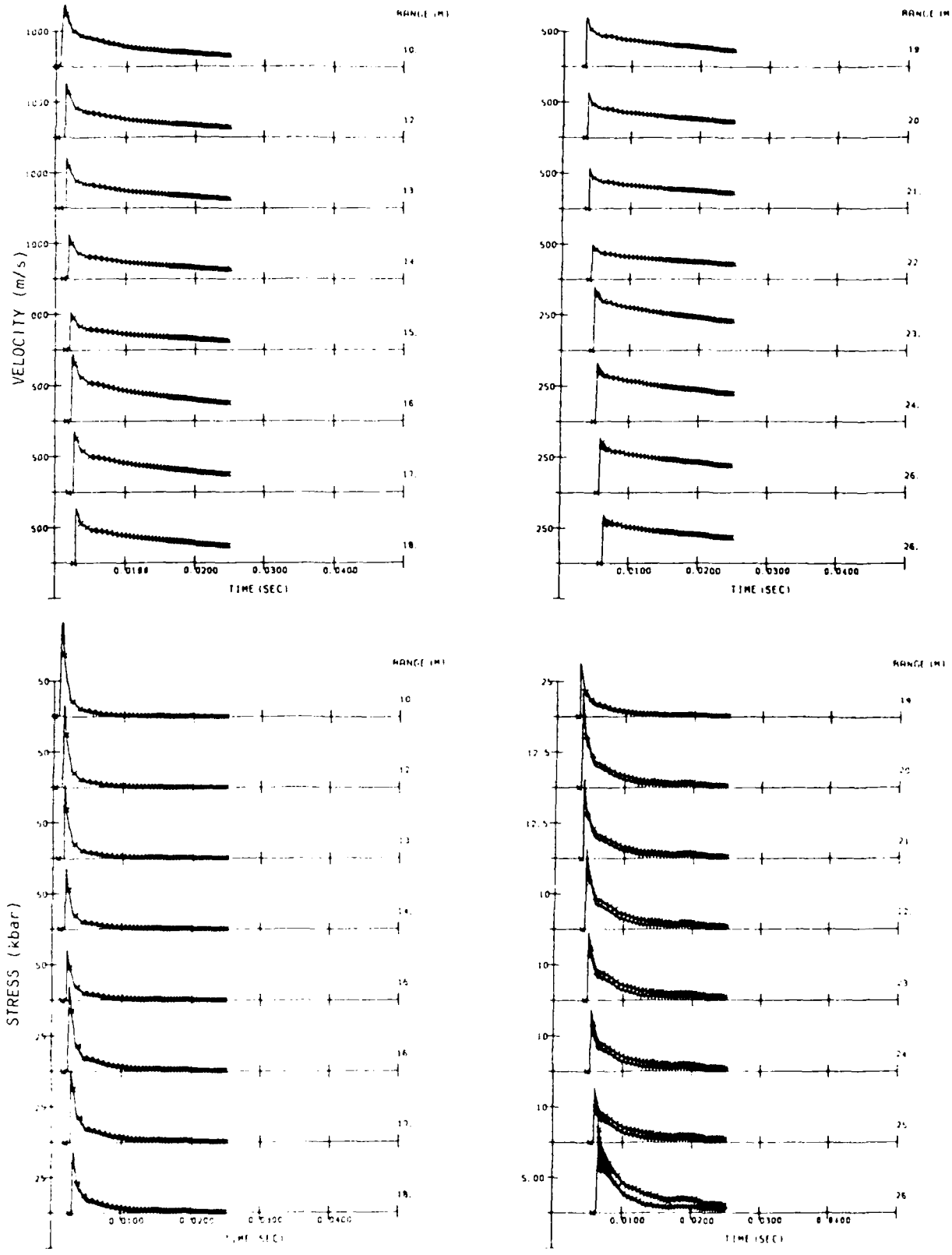

Figure 7. Spherical 1-D calculation, 15.5 kt yield.

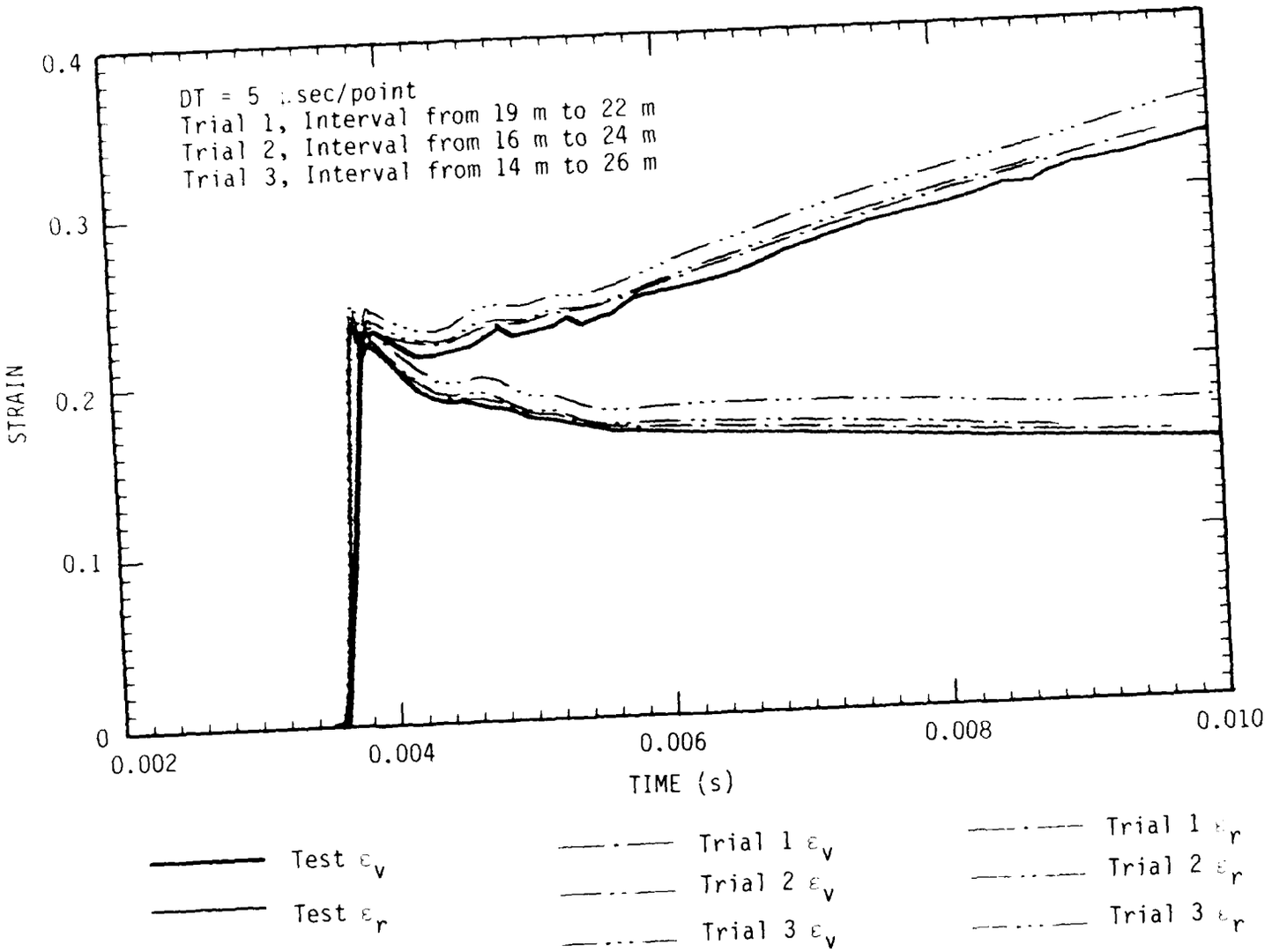

Figure 8. Comparison of Lagrangian strain estimation with CRALE 1-D spherical nuclear contained.

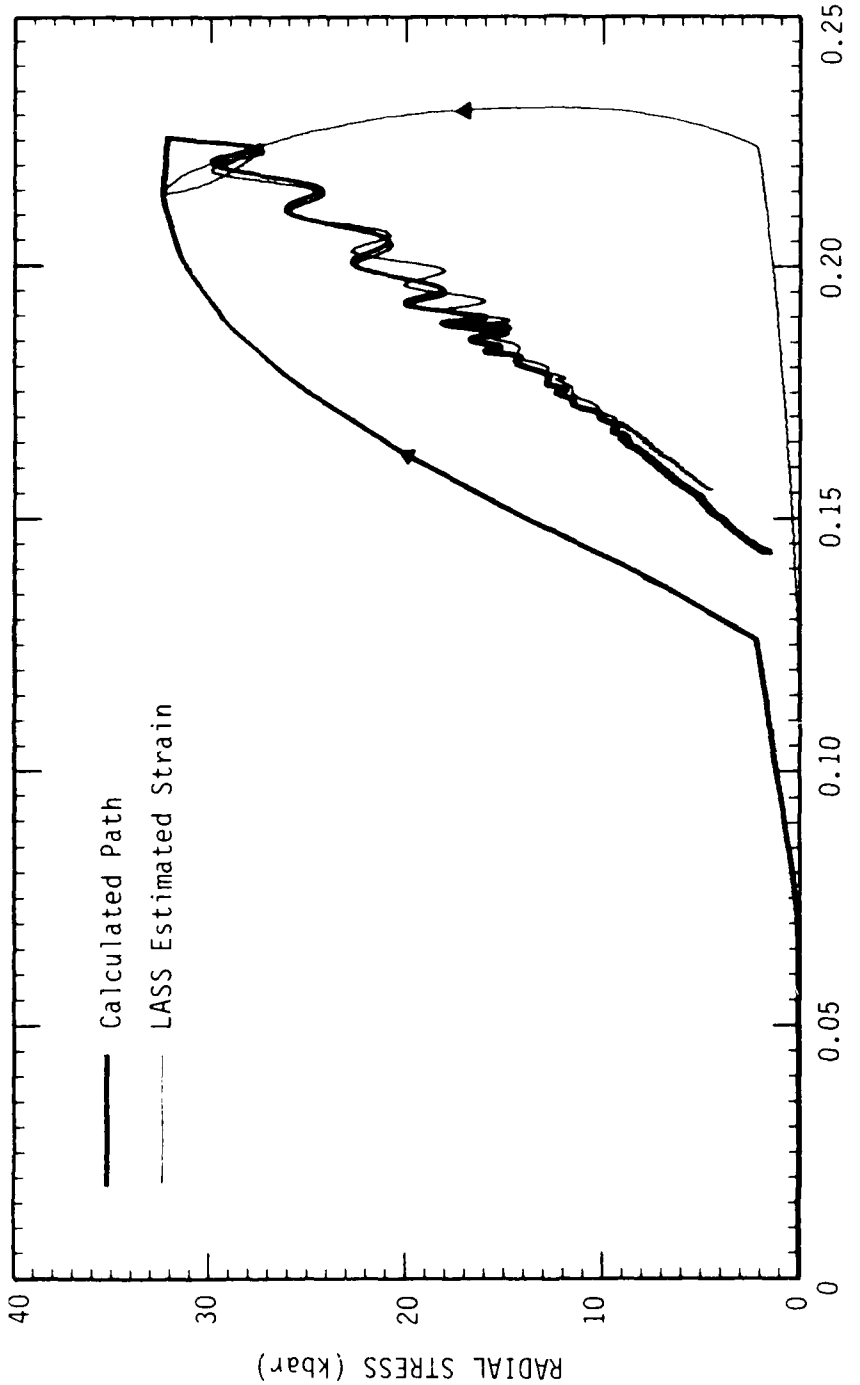

Figure 9. Effect of 60 μsec timing error on material model estimation. See text for differences in loading.

The source of error is due entirely to the discrete zone size used. This allowed velocity (and, hence, strains estimated from velocity) to rise to peak more quickly than compression, which required the shock front to traverse the zone completely. In this case, the difference in timing that produced such a completely invalid material model estimation was 60 μsec, or about ten calculational cycles.

The lesson learned above, that small errors in estimated strains lead to extremely large errors in model estimation, applies in practice in a somewhat different manner. We can note that gage rise times play a singular role in determining the accuracy of an estimated material model.

SECTION 9
SENSITIVITY OF ϵ_v TO BASELINE CORRECTIONS APPLIED TO VELOCITY RECORDS

It is important to investigate the effect of baseline corrections because:

1. Some sort of velocity drift correction is inevitably applied to integrated accelerometer records, and

2. Such a correction implies a direct effect on so-called observed radial displacements, and ϵ_t, ϵ_r, and ϵ_v are all functions of this displacement and partials thereof.

Consider ϵ_v at some fixed time after arrival of motion. Then, by definition:

$$\epsilon_v = 1 - \left(\frac{r}{h}\right)^2 \cdot \frac{\partial r(h,t)}{\partial h}.$$

Then write r as:

$$r(h,t_o) = h + \int_{f(h)}^{t_o} u(h,t)dt = h + D(h,t_o), \tag{37}$$

where D is the displacement at the fixed time. Thus, ϵ_v is now a function of the independent variables h and D. Then:

$$\epsilon_v = 1 - \left[1 + \frac{\partial D}{\partial h}\right] \cdot \left[1 + \frac{D}{h}\right]^2 \tag{38}$$

Changes in ϵ_v due to small changes in h (due to positional errors) and D (due to baseline shifts) are given by

$$\Delta\epsilon_v = \Delta D \cdot \frac{\partial}{\partial D}\{\epsilon_v(h,D)\}_{h_o,D_o} + \Delta h \cdot \frac{\partial}{\partial h}\{\epsilon_v(h,D)\}_{h_o,D_o}. \qquad (39)$$

This is the equation of the tangent plane at (h_o,D_o).

$$\Delta\epsilon_v = \Delta D \cdot \left(1 + \frac{D_o}{h_o}\right)\left[\left(1 + \frac{D_o}{h_o}\right)\left(\frac{\partial D}{\partial h}\right)^2 \frac{\partial^2 h}{\partial D^2} + \right.$$

$$\left. \frac{2}{h_o} \cdot \left(\frac{D_o}{h_o} - 1\right) + \frac{2}{h_o}\left(\frac{D_o}{h_o \cdot \frac{\partial D}{\partial h}} - \frac{\partial D}{\partial h}\right)\right] \qquad (40)$$

$(\Delta h = 0)$

This expression is difficult to evaluate fully. In order to evaluate it qualitatively, assume $1 + D_o/h_o$ is approximately 1, which it will be for early times.[11] Then:

$$\Delta\epsilon_v = \Delta D \cdot \left[\left(\frac{\partial D}{\partial h}\right)^2 \frac{\partial^2 h}{\partial D^2} + \frac{2}{h_o} + \frac{2}{h_o}\left(\frac{D_o}{h_o \cdot \frac{\partial D}{\partial h}} - \frac{\partial D}{\partial h}\right)\right] \qquad (41)$$

---

11 This will prove to be a valid operation, since these terms are greater than zero. It also removes the stipulation for earlier times.

Therefore,[12]

$$\epsilon_v - \epsilon_{vo} = (D - D_o) \cdot (\text{positive number})$$

$$D > D_o \rightarrow \epsilon_v > \epsilon_{vo}, \tag{42}$$

that is, a baseline shift that gives higher displacements for the central gage at some time works to give a greater volumetric strain at the same time. An example of this type of error is shown in Figure 10. Other baseline shifts for the two end gages can also be calculated.

This result has the important implications that positive baseline correction (a correction which gives a high displacement) works to keep ϵ_v (and hence μ) higher in magnitude than it actually is. Then, the strain-time history, in conjunction with an accepted stress-time record,[13] would tend to indicate an abnormally high unload modulus or even a negative unload modulus, "competency," or the continued compaction of material with falling pressure.

A drift correction of opposite magnitude (giving displacements that are too small) would tend to indicate

---

12 The term $\partial^2 h/\partial D^2$ is asymptotic to and always greater than zero; at early times it will be very large. This can be seen by noting that the graph of h versus D in a divergent field will be a power law curve upwardly concave. $\partial h/\partial D$ will, therefore, always be negative and upwardly convex. Note also that $\partial D/\partial h$ will be a relatively large negative number; hence, the first term in the last parentheses is neglected. The statement follows easily from these arguments.

13 An assumption here being that the times-of-arrival of the stress and velocity records are identical.

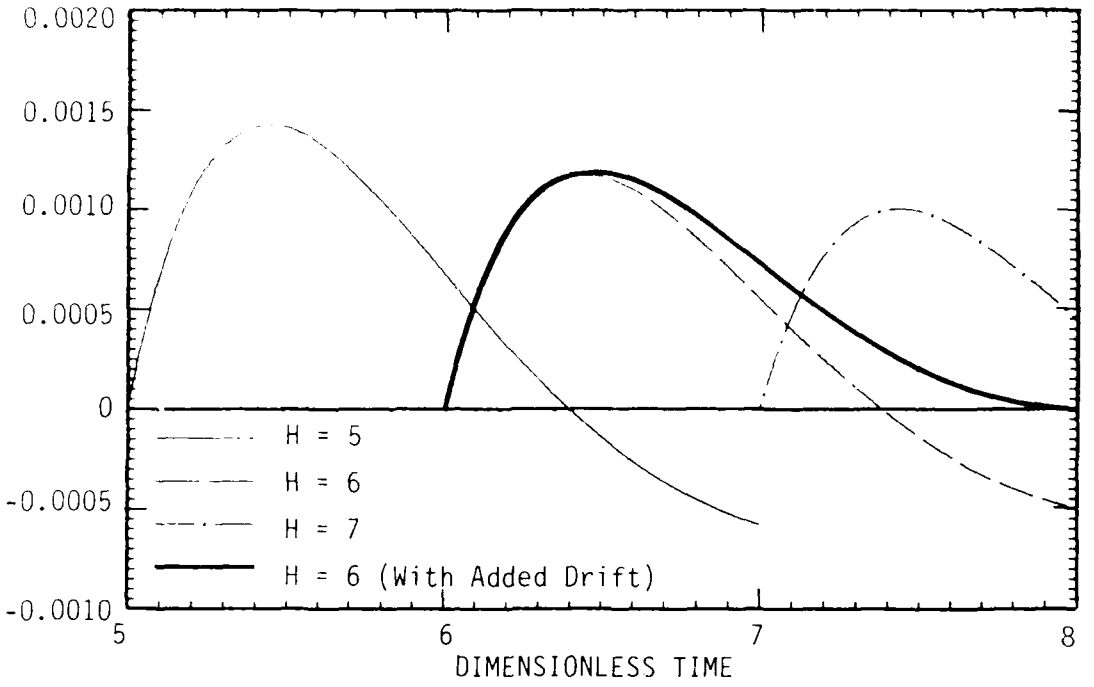

Figure 10a. Velocity records from closed form spherical 1-D problem (Grady).

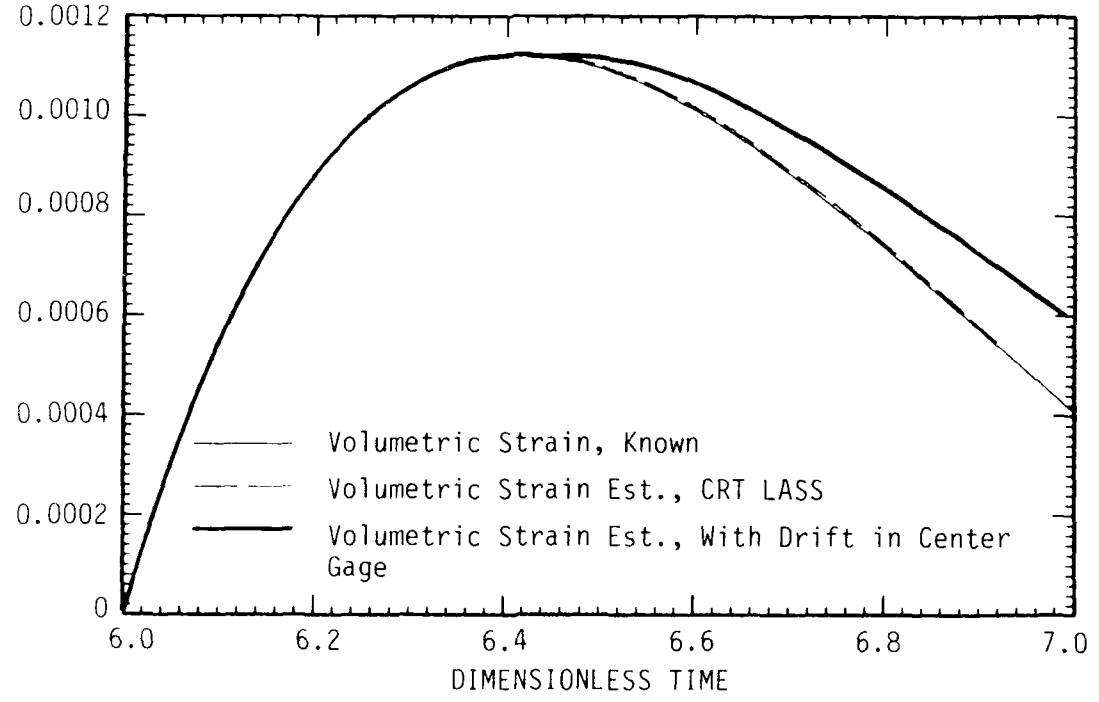

Figure 10b. Effect of baseline shift applied to known center velocity gage.

excessive "dilatancy" during stress relief--too much unload recovery.

The following two statements are especially pertinent in materials that unload very little, such as dry soils, where the slope of volumetric strain is very shallow with respect to time.

Linear baseline corrections are inevitably applied upon shock passage; if incorrect,[14] such corrections thus give resultant displacements that become increasingly in error with the passage of time. Volumetric material behavior on unload derived from Equation 24 is, thus, immediately subject to a doubt that grows with the degree of unloading. The degree of error is unknown unless the velocity records are known a priori to be correct. Tentatively correct corrections, of course, imply tentatively correct strains which, therefore, must be verified by other methods.

It might also be noted that "averaging" records in a neighborhood in an attempt to cull a more accurate record is incorrect unless it is known that the distribution of gage drifts is uniformly random about zero. (For example, an average of three records in a neighborhood cannot produce a better approximation than any one of the individual records if all three gages require systematic positive drift corrections during unload.)

---

14 Frequently, more than one correction is possible, especially when like-gage responses are compared.

SECTION 10

LIST OF REFERENCES

1. Grady, D. E., "Experimental Analysis of Spherical Wave Propagation," Journal of Geophysical Research, Vol. 78, No. 8, March 10, 1973, pp. 1299-1307.

2. Fowles, R., Williams, R.F., "Plane Stress Wave Propagation in Solids," Journal of Applied Physics, Vol. 41, No. 1, January 1970, pp. 360-363.

3. Seamen, L., "Lagrangian Analysis For Multiple Stress or Velocity Gages in Attenuating Waves," Journal of Applied Physics, Vol. 45, No. 10, October 1974, pp. 4303-4314.

4. Grady, D.E., et al., "In Situ Constitutive Relations of Soils and Rocks," Stanford Research Institute Interim Report, March 1974, DNA 3671Z.

5. Trulio, J.G., "Strain Path Modeling for Geomaterials," DNA-TR-84-105, Final Report for Defense Nuclear Agency, Applied Theory, Inc., March 1984.

6. Trulio, J.G., "In Situ Strain Paths and Stress Bounds With Applications to Desert Alluvium, DNA-TR-84-310, Technical Report for Defense Nuclear Agency, Applied Theory, Inc., July 31, 1984.

7. Kitch, W.A., et al., "Material Properties Test No. 2: Data Report," AFWL-TR-85-44, Air Force Weapons Laboratory, Kirtland AFB, NM March 1987.

8. Rinehart, E.J., Veyera, G.E., "MP2 Review and Final Data Analysis, CRTA-3751F, California Research & Technology, Inc., Albuquerque, NM, September 1986.

9. Presentations from the MP-2 Analysis Review Meeting, R & D Associates, Marina del Rey, CA, June 5, 1985

10. Allen, R.T., M.B. Fogel, and C.C. Swan, Jr., "Ground Motion Postdictions for the CARES MP2 Event," PT-U85-0708, Pacifica Technology, Del Mar, CA, May 1986.

11. Rinehart, E.J., G.M. Lloyd, and R.H. England, "Analysis of MILL YARD Using Lagrangian Methods (U)," CRTA-TR-3720-1, California Research & Technology, Inc., Albuquerque, NM, April 1987.

LIST OF REFERENCES (Concluded)

12. Courant, R. Friedrichs, K.O., Supersonic Flow and Shock Waves, Springer-Verlag, 1948, 1976.

13. Ahmed, N., Natarjian, T., Discrete-Time Signals and Systems, Reston Publishing Company, Inc., 1983, p. 190.

14. Dahlquist, Germund, Bjorck, Ake, Numerical Methods, Prentice Hall, 1974.

15. Kerry, P.D., Watson, A.T., "A New Algorithm for Estimating Relative Permeabilities from Displacement Experiments," Society of Petroleum Engineers, Reservoir Engineering, Volume 2, No. 1, February 1987, p. 111 (Appendix A).

16. Gonzalez-Casanova, P., Alvarez, R., "Splines in Geophysics," Geophysics, Vol. 50, No. 12, December 1985, pp. 2831-2848.

SECTION 11
LIST OF SYMBOLS

t	time
t_a	time-of-arrival at a particular Lagrangian position
ρ_o	initial material density
h	Lagrangian position
h_f	Lagrangian position of wave front at time, t
h_g	Lagrangian position of particle at zero time
r	Eulerian position
u	velocity of Lagrangian particle at h and t
$\dot{u}$	acceleration
σ_r	radial stress
σ_t	tangential stress
x,y	transformed time and Lagrangian position coordinates
$\tilde{u}(x,y)$	local fitting function in transformed coordinates
ϵ_t	tangential strain
ϵ_r	radial strain
ϵ_v	volumetric strain
μ	excess compression
κ	stress difference
a_1,a_2,a_3,b_1,b_2,b_3	fitting constants
σ^L	lower radial stress bound
σ^U	upper radial stress bound
θ	tensile limit of material

DISTRIBUTION LIST

DEPARTMENT OF DEFENSE

AFSOUTH
ATTN: U S DOCUMENTS OFFICER

ARMED FORCES STAFF COLLEGE
ATTN: LIBRARY

ASSISTANT SEC OF DEF (C31)
ATTN: DASD(I)

ASSISTANT TO THE SECRETARY OF DEFENSE
ATOMIC ENERGY
ATTN: EXECUTIVE ASSISTANT

COMMANDER IN CHIEF, PACIFIC
ATTN: IPAC/PT
ATTN: J-3
ATTN: J-32
ATTN: J-54
ATTN: J-634
ATTN: J-64

DEFENSE INTELLIGENCE AGENCY
ATTN: DB
ATTN: DB-1/RCH SOV WPN DIV/G FERRELL
ATTN: DB-6/RCH TGT INTELL DIV/R MANN
ATTN: DE(ESTIMATES)
ATTN: DI-5
ATTN: DIA/VPA-2 (FED RES DIV)
ATTN: DT-1B
2 CYS ATTN: RTS-2B
ATTN: RTS-2C (TECH SVCS & SPT)

DEFENSE NUCLEAR AGENCY
ATTN: DFRA
ATTN: NANF
ATTN: NASF
ATTN: NAWE
ATTN: OPNA
ATTN: OPNS
ATTN: RAEE
4 CYS ATTN: TITL

DEFENSE TECHNICAL INFORMATION CENTER
12CYS ATTN: DD

DIRECTOR
ATTN: DOCUMENT CONTROL

FIELD COMMAND DEFENSE NUCLEAR AGENCY
ATTN: FCTXE
ATTN: FTTD W SUMMA

INTELLIGENCE CENTER, PACIFIC
ATTN: COMIPAC

JOINT CHIEFS OF STAFF
ATTN: ED30/J-3 STRAT OPS DIV
ATTN: J-3 STRAT OPERATIONS DIV
ATTN: J-5 NUCLEAR & CHEM DIV
3 CYS ATTN: J-5 NUC DIV/STRAT DIV/FP&P DIV
ATTN: JAD
ATTN: JAD/SFD
ATTN: JAD/SSD

JOINT DATA SYSTEM SUPPORT CTR
ATTN: C-312 R MASON
ATTN: C-332

JOINT STRAT TGT PLANNING STAFF
2 CYS ATTN: JK (ATTN: DNA REP)
ATTN: JKCS
ATTN: JLT
ATTN: JP
ATTN: JPEP

LAWRENCE LIVERMORE NATIONAL LABORATORY
ATTN: DNA-LL

NATIONAL DEFENSE UNIVERSITY
ATTN: ICAF-ICC
ATTN: NWCO

NATIONAL SECURITY AGENCY
ATTN: A12 F NEWTON
ATTN: CHIEF A GROUP

OFFICE OF THE SEC OF DEFENSE
ATTN: NAVAL FORCES
2 CYS ATTN: STRATEGIC PROGRAMS & TNF

STRATEGIC AND THEATER NUCLEAR FORCES
ATTN: DR WOODRUFF

U S EUROPEAN COMMAND/ECC3S-CCN
ATTN: ECC3S-CCN

U S EUROPEAN COMMAND/ECJ-LW
ATTN: ECJ-LW

U S EUROPEAN COMMAND/ECJ-2-ITD
ATTN: ECJ-2-ITD

U S EUROPEAN COMMAND/ECJ-3
ATTN: ECJ-3

U S EUROPEAN COMMAND/ECJ2-T
ATTN: ECJ2-T/TGTS DIV

U S EUROPEAN COMMAND/ECJ5-N
ATTN: ECJ5-N/NUC BRANCH

U S NATIONAL MILITARY REPRESENTATIVE
ATTN: U S DOCUMENTS OFFICER

UNDER SEC OF DEFENSE FOR POLICY
ATTN: DUSP/P
ATTN: USD/P

UNDER SECRETARY OF DEFENSE
ATTN: DEP UND SEC/TAC WARFARE PGMS
ATTN: STRAT & SPACE SYS(OS)
ATTN: STRAT & THEAT NUC FOR F VAJDA

DEPARTMENT OF THE ARMY

DEP CH OF STAFF FOR OPS & PLANS
ATTN: DAMO-NCN
ATTN: DAMO-NCN(NUC CHEM DIR)
ATTN: DAMO-RQS
ATTN: DAMO-ZXA

DEP CH OF STAFF FOR RSCH DEV & ACQ
ATTN: DAMA-CSM-N

EIGHTH U S ARMY
ATTN: EACJ-PON-NS

HARRY DIAMOND LABORATORIES
ATTN: SCHLD-NW-P
ATTN: SLCIS-IM-TL (TECH LIB)

U S ARMY AIR DEFENSE SCHOOL
ATTN: COMMANDANT

U S ARMY ARMOR SCHOOL
ATTN: ATSB-CTD
ATTN: TECH LIBRARY

U S ARMY BALLISTIC RESEARCH LAB
ATTN: SLCBR-DD-T
ATTN: SLCBR-SS-T (TECH LIB)

U S ARMY COMB ARMS COMBAT DEV ACTY
ATTN: ATZL-CAP

U S ARMY COMD & GENERAL STAFF COLLEGE
ATTN: ACQ LIBRARY DIV
ATTN: ATSW-TA-D

U S ARMY EUROPE AND SEVENTH ARMY
ATTN: AEAGC

U S ARMY INFANTRY CTR & SCH
ATTN: ATSH-CD-CS

U S ARMY MATERIEL COMMAND
ATTN: AMCCN

U S ARMY MATERIEL SYS ANALYSIS ACTVY
ATTN: AMXSY-CR

U S ARMY MISSILE COMMAND
ATTN: AMSMI-XF

U S ARMY NUCLEAR & CHEMICAL AGENCY
ATTN: LIBRARY

U S ARMY STRATEGIC DEFENSE CMD
ATTN: DACS-BM/J KAHLAS

U S ARMY TRADOC SYS ANALYSIS ACTVY
ATTN: ATRC-TD

U S ARMY WAR COLLEGE
ATTN: LIBRARY

USA MILITARY ACADEMY
ATTN: DOCUMENT LIBRARY

V CORPS
ATTN: COMMANDER
ATTN: G-3

VII CORPS
ATTN: G-3

DEPARTMENT OF THE NAVY

CARRIER AIRBORNE EARLY WARNING WING 12
ATTN: COMMANDER

CARRIER GROUP 1
ATTN: COMMANDER

CARRIER GROUP 2
ATTN: COMMANDER

CARRIER GROUP 3
ATTN: COMMANDER

CARRIER GROUP 4
ATTN: COMMANDER

CARRIER GROUP 5
ATTN: COMMANDER

CARRIER GROUP 7
ATTN: COMMANDER

CARRIER GROUP 8
ATTN: COMMANDER

CRUISER DESTROYER GROUP ONE
ATTN: COMMANDER

CRUISER-DESTROYER GROUP 12
ATTN: COMMANDER

CRUISER-DESTROYER GROUP 2
ATTN: COMMANDER

CRUISER-DESTROYER GROUP 3
ATTN: COMMANDER

CRUISER-DESTROYER GROUP 5
ATTN: COMMANDER

CRUISER-DESTROYER GROUP 8
ATTN: COMMANDER

DAVID TAYLOR NAVAL SHIP R & D CTR
ATTN: CODE 174

FIGHTER AIRBORNE EARLY WARNING WING
ATTN: COMMANDER

FIGHTER WING 1
ATTN: COMMANDER

FLEET INTELLIGENCE CTR EUROPE & ATLANTIC
ATTN: LIBRARY CODE 113

LIGHT ATTACK WING
ATTN: COMMANDER

MARINE CORPS DEV & EDUCATION COMMAND
ATTN: COMMANDER

MEDIUM ATTACK TACTICAL ELECTRONIC
ATTN: COMMANDER

NAVAL AIR FORCE
ATTN: COMMANDER

NAVAL AIR FORCE
ATTN: COMMANDER

NAVAL INTELLIGENCE SUPPORT CTR
ATTN: NISC-30

NAVAL OCEAN SYSTEMS CENTER
ATTN: CODE 9642/TECH LIB

NAVAL POSTGRADUATE SCHOOL
ATTN: CODE 1424 LIBRARY

NAVAL RESEARCH LABORATORY
ATTN: CODE 1220
ATTN: CODE 2627/TECH LIB

NAVAL SEA SYSTEMS COMMAND
ATTN: SEA-09G53 (LIB)
ATTN: SEA-643

NAVAL SURFACE FORCE
ATTN: COMMANDER

NAVAL SURFACE FORCE
ATTN: COMMANDER

NAVAL WEAPONS EVALUATION FACILITY
ATTN: CLASSIFIED LIBRARY

NUCLEAR WEAPONS TNG GROUP, ATLANTIC
ATTN: CODE 221
ATTN: DOCUMENT CONTROL

NUCLEAR WEAPONS TNG GROUP, PACIFIC
ATTN: DOCUMENT CONTROL

OFC OF THE DEPUTY CHIEF OF NAVAL OPS
ATTN: OP 654/TRAT EVAL & ANAL BR
ATTN: OP 955(AAW DIV)
ATTN: OP 981

OFFICE OF THE CHIEF OF NAVAL OPERATIONS
ATTN: CNO EXEC PANEL/OP-00K

OPERATIONAL TEST & EVALUATION FORCE
ATTN: CODE 80

OPERATIONAL TEST & EVALUATION FORCE,
ATTN: INTEL OFFICER

SUBMARINE FORCE
ATTN: COMMANDER

SUBMARINE GROUP 6
ATTN: COMMANDER

TACTICAL TRAINING GROUP, PACIFIC
ATTN: COMMANDER

TACTICAL WINGS ATLANTIC
ATTN: COMMANDER

THEATER NUCLEAR WARFARE PROGRAM OFC
ATTN: PMS 423

U S NAVAL FORCES, EUROPE
ATTN: N54, NUC WARFARE OFCR

U S NAVY SEVENTH FLEET
ATTN: COMMANDER

U S NAVY SIXTH FLEET
ATTN: COMMANDER

DEPARTMENT OF THE AIR FORCE

AF/INE
ATTN: INA

AFIS/INT
ATTN: INT

AIR FORCE SYSTEMS COMMAND
ATTN: DL
ATTN: SD

AIR FORCE WEAPONS LABORATORY
ATTN: SUL

AIR UNIVERSITY LIBRARY
ATTN: AUL-LSE

ASSISTANT CHIEF OF THE AIR FORCE
ATTN: SAF/ALR

DEPUTY CHIEF OF STAFF/AF-RDQM
ATTN: AF/RDQI

DEPUTY CHIEF OF STAFF/XOO
ATTN: AF/XOC

DEPUTY CHIEF OF STAFF/XOX
ATTN: AFXOXFM/PLNS, FRC DEV MUN PLNS
ATTN: AFXOXFS/FRC DEV, STRAT OFF FRC

SPACE DIVISION/CWH
ATTN: CWH (DSCS 111)

STRATEGIC AIR COMMAND/NRI-STINFO
ATTN: NRI/STINFO

STRATEGIC AIR COMMAND/STIC
ATTN: STIC (544SIW)

TACTICAL AIR COMMAND TAC/DOA
ATTN: TAC/DOA

TACTICAL AIR COMMAND/XPJ
ATTN: TAC/XPJ

U S AIR FORCES IN EUROPE/DEX
ATTN: USAFE/DEXX

U S AIR FORCES IN EUROPE/DOT
ATTN: USAFE/DOQ

U S AIR FORCES IN EUROPE/INAT
ATTN: USAFE/INAT

2ND ACCS
ATTN: DOC

DEPARTMENT OF ENERGY

DEPARTMENT OF ENERGY
ATTN: OMA, DP 22

LAWRENCE LIVERMORE NATIONAL LAB
ATTN: L-35
ATTN: L-38
ATTN: L-389
ATTN: L-450 W HOGAN
ATTN: L-53 TECH INFO DEPT LIB
ATTN: Z DIVISION LIBRARY

LOS ALAMOS NATIONAL LABORATORY
ATTN: D RICHMOND
ATTN: F601 T DOWLER
ATTN: MS P364 REPORT LIBRARY
ATTN: R SANDOVAL

SANDIA NATIONAL LABORATORIES
ATTN: TECH LIB 3141/RPTS RCVG CLRK
ATTN: 0333 R B STRATTON

OTHER GOVERNMENT

CENTRAL INTELLIGENCE AGENCY
ATTN: N10 - STRATEGIC SYS

FEDERAL EMERGENCY MANAGEMENT AGENCY
ATTN: G ORRELL NP-CP
ATTN: OFC OF RSCH/NP H TOVEY

U S DEPARTMENT OF STATE
ATTN: PM/TMP

DEPARTMENT OF DEFENSE CONTRACTORS

ADVANCED RESEARCH & APPLICATIONS CORP
ATTN: DOCUMENT CONTROL

BDM CORP
ATTN: C WASAFF
ATTN: J BODE
ATTN: J BRADDOCK
ATTN: R BUCHANAN

BOEING CO
ATTN: H WICKLEIN
ATTN: J W RUSSELL

CALIFORNIA RESEARCH AND TECHNOLOGY, INC
2 CYS ATTN: E RINEHART
2 CYS ATTN: G LLOYD

COMPUTER SCIENCES CORP
ATTN: F EISENBARTH

GRUMMAN-CTEC, INC
ATTN: S SHRIER

HORIZONS TECHNOLOGY, INC
ATTN: J PALMER

IIT RESEARCH INSTITUTE
ATTN: DOCUMENTS LIBRARY

INSTITUTE FOR DEFENSE ANALYSES
ATTN: CLASSIFIED LIBRARY
ATTN: J GROTE

JAYCOR
ATTN: R SULLIVAN

KAMAN SCIENCES CORP
ATTN: F SHELTON

KAMAN SCIENCES CORP
ATTN: E CONRAD

KAMAN SCIENCES CORPORATION
ATTN: DASIAC

KAMAN TEMPO
ATTN: DASIAC

MARTIN MARIETTA DENVER AEROSPACE
ATTN: J DONATHAN

ORION RESEARCH INC
ATTN: J E SCHOLZ

PACIFIC-SIERRA RESEARCH CORP
ATTN: H BRODE, CHAIRMAN SAGE

PACIFIC-SIERRA RESEARCH CORP
ATTN: D GORMLEY

R & D ASSOCIATES
ATTN: C K B LEE
ATTN: D SIMONS
2 CYS ATTN: DOCUMENT CONTROL
ATTN: F A FIELD

R & D ASSOCIATES
ATTN: A DEVERILL
ATTN: C KNOWLES
ATTN: J THOMPSON

RAND CORP
ATTN: P DAVIS
ATTN: V JACKSON

RAND CORP
ATTN: B BENNETT

ROCKWELL INTERNATIONAL CORP
ATTN: J HOWE

S-CUBED
ATTN: B PYATT

SCIENCE APPLICATIONS INTL CORP
ATTN: DOCUMENT CONTROL
ATTN: E SWICK
ATTN: J MARTIN
ATTN: M DRAKE
ATTN: R J BEYSTER

SCIENCE APPLICATIONS INTL CORP
ATTN: J SHANNON
ATTN: L GOURE
ATTN: W LAYSON

SCIENCE APPLICATIONS INTL CORP
ATTN: D KAUL

SCIENCE APPLICATIONS INTL CORP
ATTN: R CRAVER

TRW INC
ATTN: D SCALLY
ATTN: R BURNETT

END
DATED
FILM
8-88
DTIC